POLITECNICO DI TORINO
Repository ISTITUZIONALE

Modeling and Analysis of FunctionallyGraded Beams, Plates and Shells,Guest Editorial,

(Article begins on next page)

29 March 2023

Refined and Advanced Models for Multilayered Plates and Shells Embedding Functionally Graded Material Layers

E. Carrera[a]; S. Brischetto[a]; M. Cinefra[a]; M. Soave[a]

[a] Department of Aeronautics and Space Engineering, Politecnico di Torino, Italy

Online publication date: 25 November 2010

PLEASE SCROLL DOWN FOR ARTICLE

Taylor & Francis
Taylor & Francis Group

Refined and Advanced Models for Multilayered Plates and Shells Embedding Functionally Graded Material Layers

E. Carrera, S. Brischetto, M. Cinefra, and M. Soave

Department of Aeronautics and Space Engineering, Politecnico di Torino, Italy

The present work investigates the static response problem of multilayered plates and shells embedding functionally graded material (FGM) layers. Carrera's unified formulation (CUF) is employed to obtain several hierarchical refined and advanced two-dimensional models for plates and shells. The refined models are based on the principle of virtual displacements. The advanced models, based on Reissner's mixed variational theorem, permit the transverse shear and normal stresses to be "a priori" modelled. Refined and advanced models are developed in both equivalent single layer and layer wise multilayer approaches. CUF is also employed to describe the continuous variation of elastic properties in the thickness direction for the embedded FGM layers. The numerical results, which are restricted to simply supported plates/shells loaded by a harmonic distribution of transverse pressure, show that the use of refined and advanced models, based on CUF, is mandatory with respect to the classical theories that are widely employed for isotropic and one-layered structures. Furthermore, advanced models lead to a quasi-3D description of the bending problem for FGM plates and shells. New benchmarks are considered in order to investigate the possible benefits of introducing FGM layers into common multilayered structures. It has been concluded that significant benefits can be obtained by employing opportune values for κ-h_{FGM} parameters, where κ is the exponent of the thickness law for the FGM elastic properties and h_{FGM} is the thickness of the embedded FGM layers.

1. INTRODUCTION

Functionally Graded Materials (FGMs) are multiphase composites where the volume fraction of phases continuously varies through one or more directions. They are composite materials with a microscopically inhomogeneous character [1]. The concept of functionally graded materials was first proposed in 1984 by materials scientists in the Sendai area (Japan) as a

means of preparing thermal barrier materials [2]. Birman and Byrd [3] have presented a review on the principal developments in functionally graded materials, with emphasis on the recent works published since 2000. Diverse areas, relevant to various aspects concerning theory and applications of FGMs, were dealt with in this paper: homogenization of particulate FGMs, heat transfer issues, stress, stability and dynamic analyses, testing, manufacturing and design, applications, and fracture [4, 5]. Continuous changes in the composition, microstructure and porosity of these materials result in gradients in these properties such as mechanical strength and thermal conductivity. Due to these features, FGMs can be employed in several applications [6]: as an alternative to composite materials, for a new concept of sandwich structures, as thermal protection components and thermal protection systems, for wear-resistant coatings and electrically insulating joints, and as material for components in biomedical applications and the computer circuit industry. This large number of applications implies the necessity of an exhaustive analysis of structures embedding functionally graded materials. In recent years, several works have been devoted to the development of accurate structural models for FGM plates and shells.

Kashtalyan [7] has proposed a three-dimensional elasticity solution for a simply supported functionally graded plate subjected to a transverse mechanical loading; the developed approach made use of the Plevako general solution [8] of the equilibrium equations for inhomogeneous isotropic media. This three-dimensional solution has been extended to sandwich plates by Kashtalyan and Menshykova [9]: the use of a functionally graded core in the sandwich panel design permits an increase in the resistance of such panels to delamination. Pan [10] has developed a three-dimensional solution for anisotropic, linearly elastic and functionally graded composite laminates under simply supported edge conditions and subjected to a mechanical load. The solutions were expressed in an elegant formalism that resembles the Stroh formalism [11], and the composite laminates can be made of multilayered, functionally graded materials with their properties varying exponentially in the thickness direction. The proposed solution extended Pagano's solutions [12, 13] to functionally graded materials. Elastic solutions for axisymmetric rotating disks, made of functionally

graded material with variable thickness, have been given in [14]. The material properties and disk thickness profile were assumed to be represented by two power-law distributions; both analytical and semi-analytical solutions are given under free-free and fixed-free boundary conditions. Zenkour [15] has proposed a generalized shear deformation theory for the static response of a simply supported, functionally graded rectangular plate subjected to a transverse uniform mechanical load. A third-order shear deformation theory has been developed by Ferreira et al. [16] for the static analysis of an FGM plate made of two isotropic constituents; collocation multiquadric radial basis functions were used. Ramirez et al. [17] decided to study the static analysis of FGM plates, considering the variable properties in the layer by means of a discrete layer approach. Chi and Chung [18] have extended the classical lamination theory, previously developed for classical laminated plates, to functionally graded plates; several results about the finite element method were given in the second part of the aforementioned paper [19]. Other interesting works about the mechanical analysis of FGM structures also consider dynamic analysis, see for example Qian et al. [20], where static and dynamic deformations of functionally graded plates have been considered by means of a higher-order shear and normal deformable plate theory and a local meshless Petrov-Galerkin method [21]. A three-dimensional solution for the vibration of FGM plates has been given in [22], Batra and Jin [23] have developed a first order shear deformation theory via the finite element method for the same kind of problem.

The present work proposes the static analysis of one-layered and multilayered plates and shells embedding FGM layers. Several refined and advanced hierarchical two-dimensional models have been developed using Carrera's Unified Formulation (CUF) [24]. Refined models, based on the Principle of Virtual Displacements (PVD) [25], consider the displacements as primary variables. Advanced or mixed models, which make use of Reissner's Mixed Variational Theorem (RMVT) [26], a pri-

ori consider both displacements and transverse shear/normal stresses [27]. The obtained models have the order of expansion in the thickness direction, for the primary variables, as a free parameter, and these can be modelled in both Equivalent Single layer (ESL) and Layer Wise (LW) form. CUF [24, 25], which was originally developed for multilayered anisotropic plates and shells, has been extended to the static mechanical analysis of FGM plates in [28] and [29] using PVD and RMVT variational statements, respectively. Both refined and advanced models have been applied to static sandwich plate analysis in [30], in order to investigate the effects of different FGM cores embedded between a ceramic and a metallic face. The first part of this paper investigates the importance of refined and advanced models for structures embedding FGM layers. The superiority of these models is clearly demonstrated, compared with classical two-dimensional models such as the Classical Lamination Theory [31–33] and the First order Shear deformation Theory [34, 35]. Then, some benchmarks are proposed to investigate the benefits of introducing some FGM layers into common multilayered or sandwich plates and shells. In addition to the results given in [30], the shell geometry is also investigated and new FGM configurations are considered for the core in sandwich structures.

2. GEOMETRICAL RELATIONS

A thin shell is defined as a three-dimensional body bounded by two closely spaced curved surfaces, where the distance between the two surfaces must be small compared to the other dimensions. The middle surface of the shell is the locus of the points which lie midway between these surfaces. The distance between the surfaces measured along the normal to the middle surface is the *thicknes*s of the shell at that point [36]. Shells may be seen as generalizations of a flat plate [37]; conversely, a flat plate is a special case of a shell with no curvature, see Figure 1.
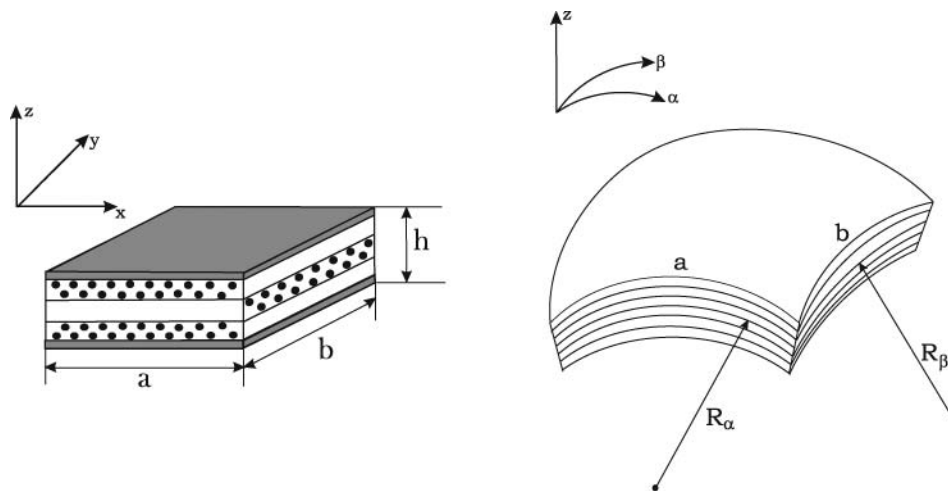

FIG. 1.   Example of a multilayered plate (on the left) and a multilayered spherical shell (on the right).

In the case of shells with constant radii of curvature, the geometrical relations are written in the following matrix form:

$$\epsilon_{pG}^k = \left[\epsilon_{\alpha\alpha}^k, \epsilon_{\beta\beta}^k, \gamma_{\alpha\beta}^k\right]^T = \left(\boldsymbol{D}_p^k + \boldsymbol{A}_p^k\right) u^k, \tag{1}$$

$$\epsilon_{nG}^k = \left[\gamma_{\alpha z}^k, \gamma_{\beta z}^k, \epsilon_{zz}^k\right]^T = \left(\boldsymbol{D}_{np}^k + \boldsymbol{D}_{nz}^k + \boldsymbol{A}_n^k\right) u^k, \tag{2}$$

where, for each layer k, the vector of displacement components is $u^k = (u^k, V^k, w^k)$. The explicit form of the introduced arrays is:

$$\boldsymbol{D}_p^k = \begin{bmatrix} \dfrac{\partial_\alpha}{H_\alpha^k} & 0 & 0 \\[2mm] 0 & \dfrac{\partial_\beta}{H_\beta^k} & 0 \\[2mm] \dfrac{\partial_\beta}{H_\beta^k} & \dfrac{\partial_\alpha}{H_\alpha^k} & 0 \end{bmatrix}, \quad \boldsymbol{D}_{np}^k = \begin{bmatrix} 0 & 0 & \dfrac{\partial_\alpha}{H_\alpha^k} \\[2mm] 0 & 0 & \dfrac{\partial_\beta}{H_\beta^k} \\[2mm] 0 & 0 & 0 \end{bmatrix},$$

$$\boldsymbol{D}_{nz}^k = \begin{bmatrix} \partial_z & 0 & 0 \\ 0 & \partial_z & 0 \\ 0 & 0 & \partial_z \end{bmatrix}. \tag{3}$$

$$\boldsymbol{A}_p^k = \begin{bmatrix} 0 & 0 & \dfrac{1}{H_\alpha^k R_\alpha^k} \\[2mm] 0 & 0 & \dfrac{1}{H_\beta^k R_\beta^k} \\[2mm] 0 & 0 & 0 \end{bmatrix}, \quad \boldsymbol{A}_n^k = \begin{bmatrix} \dfrac{1}{H_\alpha^k R_\alpha^k} & 0 & 0 \\[2mm] 0 & \dfrac{1}{H_\beta^k R_\beta^k} & 0 \\[2mm] 0 & 0 & 0 \end{bmatrix}. \tag{4}$$

In the proposed differential arrays (Eq. (3)), the symbols ∂_α, ∂_β and ∂_z indicate the partial derivatives $\frac{\partial}{\partial\alpha}$, $\frac{\partial}{\partial\beta}$, and $\frac{\partial}{\partial z}$, respectively. The matrices in Eq. (4) are the algebraic geometrical contributions for shells. The parameters H_α^k and H_β^k are:

$$H_\alpha^k = \left(1 + \frac{z^k}{R_\alpha^k}\right), \quad H_\beta^k = \left(1 + \frac{z^k}{R_\beta^k}\right). \tag{5}$$

Geometrical relations for shells degenerate into geometrical relations for plates when the radii of curvature R_α^k and R_β^k are infinite. Therefore, the parameters H_α^k and H_β^k equal 1, and the orthogonal curvilinear coordinates (α, β, z) degenerate into the rectilinear ones (x, y, z).

3. CARRERA'S UNIFIED FORMULATION

Carrera's unified Formulation (CUF) is a technique which handles a large variety of plate/shell models in a unified manner [24]. According to CUF, the governing equations are written in terms of a few fundamental nuclei which do not formally depend on the order of expansion N used in the z direction

and on the description of variables (LW or ESL) [25, 27]. The application of a two-dimensional method for plates and shells permits to express the unknown variables as a set of thickness functions depending only on the thickness coordinate z and the correspondent variables depending on the in-plane coordinates α and β. So that the generic variable $f(\alpha, \beta, z)$, for instance displacement or transverse stresses, and its variation $\delta f(\alpha, \beta, z)$ are written according to the following general expansion:

$$\boldsymbol{f}(\alpha, \beta, z) = F_\tau(z)\boldsymbol{f}_\tau(\alpha, \beta),$$
$$\delta\boldsymbol{f}(\alpha, \beta, z) = F_s(z)\delta\boldsymbol{f}_s(\alpha, \beta), \quad \text{with } \tau, s = 1, \ldots, N. \tag{6}$$

Bold letters denote arrays, (α, β) are the in-plane coordinates and z the thickness one. The summing convention with repeated indexes τ and s is assumed. The order of expansion N goes from first to higher order values, and depending on the used thickness functions, a model can be: ESL when the variable is assumed for the whole multilayer and a Taylor expansion is employed as thickness functions $F(z)$; LW when the variable is considered independent in each layer and a combination of Legendre polynomials are used as thickness functions $F(z)$. In CUF the maximum order of expansion N in z direction is fourth. In the present work displacements can be modelled in ESL or LW form, transverse stresses are always modelled in LW form.

3.1. Equivalent Single Layer Approach

The displacement $u = (u, v, w)$ is described according to ESL description if the unknowns are the same for the whole plate, see Figure 2. The z expansion is obtained via Taylor polynomials, that is:

$$u = F_0 u_0 + F_1 u_1 + \cdots + F_N u_N = F_\tau u_\tau, \tag{7}$$

$$v = F_0 v_0 + F_1 v_1 + \cdots + F_N v_N = F_\tau v_\tau, \tag{8}$$

$$w = F_0 w_0 + F_1 w_1 + \cdots + F_N w_N = F_\tau w_\tau, \tag{9}$$

with $\tau = 0, 1, \ldots, N$; N is the order of expansion that ranges from 1 (linear) to 4:

$$F_0 = z^0 = 1, \quad F_1 = z^1 = z, \ldots, F_N = z^N. \tag{10}$$

Equations (7)–(9) can be written in a vectorial form:

$$u(\alpha, \beta, z) = F_\tau(z)u_\tau(\alpha, \beta), \quad \delta u(\alpha, \beta, z) = F_s(z)\delta u_s(\alpha, \beta),$$
$$\text{with } \tau, s = 0, \ldots, N. \tag{11}$$

First order Shear Deformation Theory (FSDT) [34, 35] is obtained from an ESL model with $N = 1$, simply imposing constant transverse displacement w through the thickness. Classical Lamination Theory (CLT) [31–33] is obtained from FSDT via an opportune penalty technique which imposes an infinite shear rigidity. It is important to remember that all the ESL theories which have transverse displacement constant or linear through
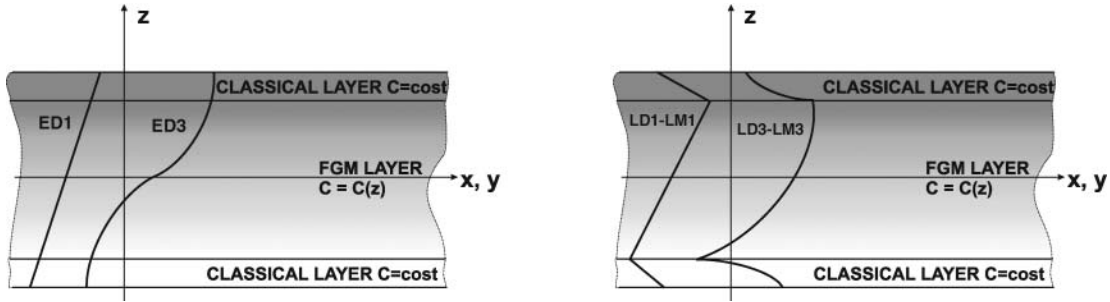
FIG. 2. Equivalent single layer theories (on the left) and layer wise theories (on the right) in multilayered plates with an FGM core.

the thickness direction, show Poisson locking phenomena; this can be overcome via plane stress conditions imposed in constitutive equations [38, 39].

The proposed ESL models do not consider the typical zigzag (ZZ) form of displacements in z direction, which is typical of multilayered structures with transverse anisotropy [40]. A remedy to this limitation can be the introduction of an opportune zigzag function in the ESL displacement model, in order to recover the ZZ form of displacements without the use of LW models. A possible choice for the zigzag function is the so-called *Murakami Zig-Zag Function* (MZZF) [41, 42]. MZZF can be simply added to displacement model and gives remarkable improvements in the solution by satisfying the typical ZZ form of displacements in multilayered structures.

The MZZF $Z(z)$ is defined according to:

$$Z(z) = (-1)^k \zeta_k, \quad (12)$$

with the not dimensioned layer coordinate $\zeta_k = (2z_k)/h_k$, where z_k is the transverse thickness coordinate and h_k is the thickness of the layer, so $-1 \leq \zeta_k \leq 1$. $Z(z)$ has the following properties: it is piece-wise linear function of layer coordinates zk; $Z(z)$ has unit amplitude for the whole layers; the slope $Z'(z) = dZ/dz$ assumes opposite sign between two-adjacent layers. Its amplitude is layer thickness independent [42].

3.2. Layer Wise Approach

When each layer of a multilayered structure is described as independent plates/shells, a Layer Wise (LW) approach is considered [27, 43]. The displacement $u^k = (u^k, v^k, w^k)$ is described for each layer k, in this way the ZZ form of displacement in multilayered transverse-anisotropy structures is easily obtained. The recovering of ZZ effect via Layer Wise models is detailed in [27, 43] and in Figure 2. The z expansion for displacement components is made for each layer k:

$$u^k = F_0\,u_0^k + F_1\,u_1^k + \cdots + F_N\,u_N^k = F_\tau\,u_\tau^k, \quad (13)$$
$$v^k = F_0\,v_0^k + F_1\,v_1^k + \cdots + F_N\,v_N^k = F_\tau\,v_\tau^k, \quad (14)$$
$$w^k = F_0\,w_0^k + F_1\,w_1^k + \cdots + F_N\,w_N^k = F_\tau\,w_\tau^k, \quad (15)$$

with $\tau = 0, 1, \ldots, N$, N is the order of expansion that ranges from 1 (linear) to 4. $k = 1, \ldots, N_l$ where N_l indicates the number of layers. The Eqs. (13–15) written in a vectorial form are:

$$u^k(\alpha, \text{ß}, z) = F_\tau(z)u_\tau^k(\alpha, \text{ß}), \quad \delta u^k(\alpha, \text{ß}, z) = F_s(z)\delta u_s^k(\alpha, \text{ß}),$$
$$\text{with} \quad \tau, s = \tau, b, \gamma \quad \text{and} \quad k = 1, \ldots, N_l, \quad (16)$$

where t and b indicate the top and bottom of each layer k, respectively; γ indicates the higher orders of expansion in the thickness direction: $\gamma = 2, \ldots, N$.

An *advanced model* considers as primary variables both displacements $\boldsymbol{u}^k = (u^k, v^k, w^k)$ and transverse shear/normal stresses $\boldsymbol{\sigma}_{nM}^k = (\sigma_{\alpha z}^k, \sigma_{\beta z}^k, \sigma_{zz}^k)$ [29]. The displacements can be modelled as ESL, ESL+MZZF and LW, and this choice permits to define the considered advanced model as ESL, ESL + MZZF or LW, respectively; the transverse shear/normal stresses $\boldsymbol{\sigma}_{nM}^k$ are always LW (the subscript M means that the stresses are a priori modelled and not obtained from the constitutive equations). The LW model for stresses is:

$$\sigma_{\alpha z}^k = F_0\sigma_{\alpha z0}^k + F_1\sigma_{\alpha z1}^k + \cdots + F_N\sigma_{\alpha zN}^k = F_\tau\sigma_{\alpha z\tau}^k, \quad (17)$$
$$\sigma_{\beta z}^k = F_0\sigma_{\beta z0}^k + F_1\sigma_{\beta z1}^k + \cdots + F_N\sigma_{\beta zN}^k = F_\tau\sigma_{\beta z\tau}^k, \quad (18)$$
$$\sigma_{zz}^k = F_0\sigma_{zz0}^k + F_1\sigma_{zz1}^k + \cdots + F_N\sigma_{zzN}^k = F_\tau\sigma_{zz\tau}^k, \quad (19)$$

The Eqs. (17)–(19) written in a vectorial form are:

$$\sigma_{nM}^k(\alpha, \text{ß}, z) = F_\tau(z)\sigma_{nM\tau}^k(\alpha, \text{ß}),$$
$$\delta\sigma_{nM}^k(\alpha, \text{ß}, z) = F_s(z)\delta\sigma_{nMs}^k(\alpha, \text{ß}), \quad \text{with} \quad \tau, s = t, b, \gamma$$
$$\text{and} \quad k = 1, \ldots, N_l. \quad (20)$$

The thickness functions $F_\tau(\zeta_k)$ and $F_s(\zeta_k)$ have now been defined at the k-layer level, they are a linear combination of Legendre polynomials $P_j = P_j(\zeta_k)$ of the jth-order defined in ζ_k-domain ($\zeta_k = \frac{2zk}{hk}$ with h_k local coordinate and h_k thickness, both referred to kth layer, so $-1 \leq \zeta_k \leq 1$). The first five

Legendre polynomials are:

$$P_0 = 1, \quad P_1 = \zeta_k, \quad P_2 = \frac{(3\zeta_k^2 - 1)}{2}, \quad P_3 = \frac{5\zeta_k^3}{2} - \frac{3\zeta_k}{2},$$
$$P_4 = \frac{35\zeta_k^4}{8} - \frac{15\zeta_k^2}{4} + \frac{3}{8}, \tag{21}$$

their combinations for the thickness functions are:

$$F_t = F_0 = \frac{P_0 + P_1}{2}, \quad F_b = F_1 = \frac{P_0 + P_1}{2},$$
$$F_\gamma = P_\gamma - P_{\gamma-2} \quad \text{with} \quad \gamma = 2, \dots, N. \tag{22}$$

The chosen functions have the following interesting properties:

$$\zeta_k = 1 \ : \ F_t = 1; \ F_b = 0; \ F_r = 0 \ at \ top, \tag{23}$$
$$\zeta_k = -1 \ : \ F_t = 0; \ F_b = 1; \ F_r = 0 \ at \ bottom. \tag{24}$$

The use of such thickness functions, thanks the property remarked in Eqs. (23) and (24), permits to easily write the Interlaminar Continuity for the transverse stresses:

$$\sigma_{nMt}^k = \sigma_{nMb}^{k+1} \quad \text{with} \quad k = 1, \dots, (N_l - 1), \tag{25}$$

that means: in each interface the top value of the layer k equals the bottom value of the layer $(k + 1)$. The same property can be used for displacements in Layer Wise form, in order to impose the compatibility conditions:

$$u_t^k = u_b^{k+1} \quad \text{with} \quad k = 1, \dots, (N_l - 1). \tag{26}$$

4. CONSTITUTIVE EQUATIONS

Constitutive equations in case of refined models are the well-known Hooke law [43]:

$$\sigma_{pC}^k = \mathbf{Q}_{pp}^k(z) \, \boldsymbol{\epsilon}_{pG}^k + \mathbf{Q}_{pn}^k(z) \, \boldsymbol{\epsilon}_{nG}^k, \tag{27}$$
$$\sigma_{nC}^k = \mathbf{Q}_{np}^k(z) \, \boldsymbol{\epsilon}_{pG}^k + \mathbf{Q}_{nn}^k(z) \, \boldsymbol{\epsilon}_{nG}^k. \tag{28}$$

Eqs. (27) and (28) are the Hooke law written in the problem reference system and split in in-plane and out-of-plane components. The vectors for the stresses are $\sigma_{pC}^k = [\sigma_{\alpha\alpha}^k, \sigma_{\beta\beta}^k, \sigma_{\alpha\beta}^k]^T$ and $\sigma_{nC}^k = [\sigma_{\alpha z}^k, \sigma_{\beta z}^k, \sigma_{zz}^k]^T$. In the case of functionally graded materials, the matrices of elastic coeffcients depend. βzzz on

the thickness coordinate z. The four sub-arrays are:

$$\mathbf{Q}_{pp}^k(z) = \begin{bmatrix} Q_{11}^k(z) & Q_{12}^k(z) & Q_{16}^k(z) \\ Q_{12}^k(z) & Q_{22}^k(z) & Q_{26}^k(z) \\ Q_{16}^k(z) & Q_{26}^k(z) & Q_{66}^k(z) \end{bmatrix},$$

$$\mathbf{Q}_{pn}^k(z) = \begin{bmatrix} 0 & 0 & Q_{13}^k(z) \\ 0 & 0 & Q_{23}^k(z) \\ 0 & 0 & Q_{36}^k(z) \end{bmatrix},$$

$$\mathbf{Q}_{np}^k(z) = \begin{bmatrix} 0 & 0 & 0 \\ 0 & 0 & 0 \\ Q_{13}^k(z) & Q_{23}^k(z) & Q_{36}^k(z) \end{bmatrix}^k, \tag{29}$$

$$\mathbf{Q}_{nn}^k(z) = \begin{bmatrix} Q_{55}^k(z) & Q_{45}^k(z) & 0 \\ Q_{45}^k(z) & Q_{44}^k(z) & 0 \\ 0 & 0 & Q_{33}^k(z) \end{bmatrix}.$$

In the case of advanced models, the constitutive equations in Eqs. (27) and (28) must be rearranged because the transverse shear/normal stresses are a priori modelled (use of subscript M):

$$\sigma_{pC}^k = \hat{\mathbf{Q}}_{pp}^k(z) \, \boldsymbol{\epsilon}_{pG}^k + \hat{\mathbf{Q}}_{pn}^k(z) \, \sigma_{nM}^k, \tag{30}$$
$$\boldsymbol{\epsilon}_{nC}^k = \hat{\mathbf{Q}}_{np}^k(z) \, \boldsymbol{\epsilon}_{pG}^k + \hat{\mathbf{Q}}_{nn}^k(z) \, \sigma_{nM}^k, \tag{31}$$

where the new coeffcients are:

$$\hat{\mathbf{Q}}_{pp}^k(z) = \mathbf{Q}_{pp}^k(z) - \mathbf{Q}_{pn}^k(z) \, \mathbf{Q}_{nn}^k(z)^{-1} \, \mathbf{Q}_{np}^k(z),$$
$$\hat{\mathbf{Q}}_{pn}^k(z) = \mathbf{Q}_{pn}^k(z) \, \mathbf{Q}_{nn}^k(z)^{-1},$$
$$\hat{\mathbf{Q}}_{np}^k(z) = -\mathbf{Q}_{nn}^k(z)^{-1} \, \mathbf{Q}_{np}(z),$$
$$\hat{\mathbf{Q}}_{nn}^k(z) = \mathbf{Q}_{nn}^k(z)^{-1}. \tag{32}$$

In the case of Functionally Graded Materials (FGMs), the properties change with continuity along a articular direction of plates and shells. In the present work elastic properties vary with continuity along the thickness direction z. The matrix of elastic coeffcients $\mathbf{Q}$ or the matrix of modified coeffcients for the RMVT case $\hat{\mathbf{Q}}$, are given for a kth FGM layer as:

$$\mathbf{Q}(z) = \mathbf{Q}_0 * f(z), \tag{33}$$
$$\hat{\mathbf{Q}}(z) = \hat{\mathbf{Q}}_0 * g(z). \tag{34}$$

The functions $f(z)$ and $g(z)$ are general continuous functions of the thickness coordinate z. The variations in z of these material properties are described via particular thickness functions, that are a combination of Legendre polynomials (see [28, 29] and Eqs. (21) and (22)). For a generic matrix $\mathbf{C}$, which can be $\mathbf{Q}(z)$ for the PVD case and $\hat{\mathbf{Q}}(z)$ for the RMVT case, it is possible to

write:

$$C(z) = F_b(z)C_b + F_\gamma(z)C_\gamma + F_t(z)C_t = F_r(z)C_r, \quad (35)$$

t and b are the top and bottom values, and γ terms denote the higher order terms of expansion. The thickness functions $F_r(\zeta_k)$ have been defined at the k-layer level, they are a linear combination of Legendre polynomials $P_j = P_j(\zeta_k)$ of the jth-order defined in Section 3.2.

In the present work a value of r equals 10 has been chosen, which always guarantees a good approximation of the FGM's properties. To obtain the C_r values, it is suficient to solve a simple algebraic system as shown in Eq. (36) for a generic component $C_{ij}(z)$:

$$\begin{bmatrix} C_{ij}(z_1) \\ \vdots \\ C_{ij}(z_{Nr}) \end{bmatrix} = \begin{bmatrix} F_b(z_1) & \cdots & F_\gamma(z_1) & \cdots & F_t(z_1) \\ \vdots & & \vdots & & \vdots \\ F_b(z_{Nr}) & \cdots & F_\gamma(z_{Nr}) & \cdots & F_t(z_{Nr}) \end{bmatrix}$$
$$\times \begin{bmatrix} C_{ijb} \\ \vdots \\ C_{ij\gamma} \\ \vdots \\ C_{ijt} \end{bmatrix} \quad (36)$$

The values of $C(z)$ and the thickness functions $F_r(z)$ are known in ten different locations along the thickness of the plate. By solving the system in Eq. (36), the values C_r are obtained. The material properties, varying with continuity in the thickness direction z, can be recovered as illustrated in Eq. (37) and in

Figure 3:

$$(C_{pp}(z), C_{pn}(z), C_{np}(z), C_{nn}(z))$$
$$= F_r(z)(C_{ppr}, C_{pnr}, C_{npr}, C_{nnr}). \quad (37)$$

By considering the approximation given in Eq. (37), it is possible to obtain a general form of constitutive relations for the PVD and RMVT case, they are valid for both cases of functionally graded materials and materials with constant properties through the thickness direction z. For the refined models, the constitutive equations are:

$$\sigma_{pC}^k = F_r Q_{ppr}^k \epsilon_{pG}^k + F_r Q_{pnr}^k \epsilon_{nG}^k, \quad (38)$$
$$\sigma_{nC}^k = F_r Q_{npr}^k \epsilon_{pG}^k + F_r Q_{nnr}^k \epsilon_{nG}^k. \quad (39)$$

In the case of advanced models, the constitutive equations state:

$$\sigma_{pC}^k = F_r \hat{Q}_{ppr}^k \epsilon_{pG}^k + F_r \hat{Q}_{pnr}^k \sigma_{nM}^k, \quad (40)$$
$$\epsilon_{nC}^k = F_r \hat{Q}_{npr}^k \epsilon_{pG}^k + F_r \hat{Q}_{nnr}^k \sigma_{nM}^k, \quad (41)$$

where $k = 1, \ldots, N_l$ indicates the considered layers, and $r = 1, \ldots, 10$ is the loop to approximate the FGM properties varying with the z coordinate. In the case of materials with constant properties in z, the loop on r index is not necessary and the material coeffcients are constant.

5. GOVERNING EQUATIONS

Governing equations are here obtained in terms of some few basic elements called fundamental nuclei. Expanding them by means of opportune indexes and loops, it is possible to obtain the matrices of the considered multilayered structures. The use
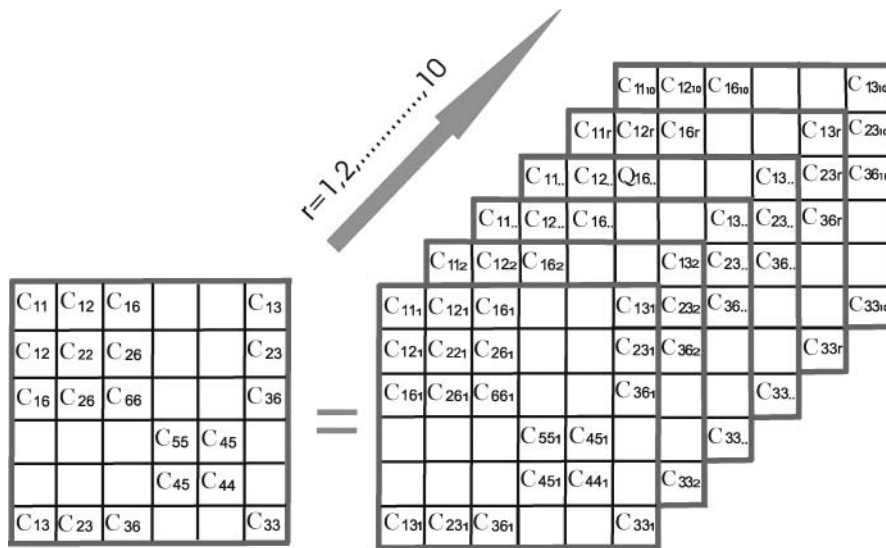

FIG. 3. Example of assembling on index r for the FGM properties.

of such nuclei permits to obtain in a unified manner several refined and advanced models which differ for the chosen order of expansion in the thickness direction (N), for the choice of the modelled variables (PVD or RMVT case), and for the multilayer description (equivalent single layer (ESL) or layer wise (LW)). Governing equations are solved in algebraic closed-form by means of Navier solution, both plate and shell geometries are considered. Refined models are based on the principle of virtual displacements (PVD) and only displacements are considered as primary variables. Advanced models are developed by means of Reissner's mixed variational theorem (RMVT) and both displacements and transverse stresses are a priori variables. Details, here omitted for sake of brevity, can be found in [28] for PVD case and in [29] for RMVT one.

5.1.   Refined Models

In the case of pure mechanical problems, the principle of virtual displacements (PVD) states as indicated:

$$\int_V \left(\delta\boldsymbol{\varepsilon}_{pG}^T \boldsymbol{\sigma}_{pC} + \delta\boldsymbol{\varepsilon}_{nG}^T \boldsymbol{\sigma}_{nC} \right) dV = \delta L_e - \delta L_{in}. \tag{42}$$

By considering a laminate of N_l layers, and the integral on the volume V_k of each layer k as an integral on the in-plane domain Ω_k plus the integral in the thickness-direction domain A_k, it is possible to write:

$$\sum_{k=1}^{N_l} \int_{\Omega_k} \int_{A_k} \left\{ \delta\boldsymbol{\varepsilon}_{pG}^k{}^T \boldsymbol{\sigma}_{pC}^k + \delta\boldsymbol{\varepsilon}_{nG}^k{}^T \boldsymbol{\sigma}_{nC}^k \right\} d\Omega_k dz$$
$$= \sum_{k=1}^{N_l} \delta L_e^k - \sum_{k=1}^{N_l} \delta L_{in}^k, \tag{43}$$

where δL_e^k and δL_{in}^k are the external and inertial virtual works at the k-layer level, respectively. The relative constitutive equations, written in order to consider the case of some functionally graded material layers embedded in the structure [28], are those obtained in Eqs. (38) and (39). By considering a generic layer k and substituting the Eqs. (38) and (39) in the variational statement of Eq. (43) (subscript C):

$$\int_{\Omega_k} \int_{A_k} \left\{ \delta\boldsymbol{\varepsilon}_{pG}^k{}^T \left(F_r \boldsymbol{Q}_{ppr}^k \boldsymbol{\varepsilon}_{pG}^k + F_r \boldsymbol{Q}_{pnr}^k \boldsymbol{\varepsilon}_{nG}^k \right) + \delta\boldsymbol{\varepsilon}_{nG}^k{}^T \right.$$
$$\left. \times \left(F_r \boldsymbol{Q}_{npr}^k \boldsymbol{\varepsilon}_{pG}^k + F_r \boldsymbol{Q}_{nnr}^k \boldsymbol{\varepsilon}_{nG}^k \right) \right\} d\Omega_k dz = \delta L_e^k - \delta L_{in}^k. \tag{44}$$

Further steps to obtain the fundamental nuclei are: the substitution of geometrical relations (subscript G), and the introduction of Carrera's unified Formulation (CUF) [24].

In Eq. (44), we can directly substitute the geometrical relations for shells as proposed in Section 2, in fact those for the plate geometry are considered as particular cases. By using the geometrical relations in Eqs. (1) and (2), the variational state-

ment is:

$$\int_{\Omega_k} \int_{A_k} \left[\left((\boldsymbol{D}_p^k + \boldsymbol{A}_p^k)\delta u^k \right)^T \left(F_r \boldsymbol{Q}_{ppr}^k (\boldsymbol{D}_p^k + \boldsymbol{A}_p^k) + F_r \boldsymbol{Q}_{pnr}^k \right. \right.$$
$$\times \left(\boldsymbol{D}_{np}^k + \boldsymbol{D}_{nz}^k - \boldsymbol{A}_n^k) \right) u^k + \left((\boldsymbol{D}_{np}^k + \boldsymbol{D}_{nz}^k - \boldsymbol{A}_n^k)\delta u^k \right)^T$$
$$\times \left(F_r \boldsymbol{Q}_{npr}^k (\boldsymbol{D}_p^k + \boldsymbol{A}_p^k) + F_r \boldsymbol{Q}_{nnr}^k (\boldsymbol{D}_{np}^k + \boldsymbol{D}_{nz}^k - \boldsymbol{A}_n^k) \right) u^k \right]$$
$$\times d\Omega_k dz = \delta L_e^k - \delta L_{in}^k. \tag{45}$$

In Eq. (45), by introducing the CUF [24] as proposed in Eq. (6):

$$\int_{\Omega_k} \int_{A_k} \left[\left((\boldsymbol{D}_p^k + \boldsymbol{A}_p^k)F_s \delta u_s^k \right)^T \left(F_r \boldsymbol{Q}_{ppr}^k (\boldsymbol{D}_p^k + \boldsymbol{A}_p^k) + F_r \boldsymbol{Q}_{ppr}^k \right. \right.$$
$$\times \left(\boldsymbol{D}_{np}^k + \boldsymbol{D}_{nz}^k - \boldsymbol{A}_n^k) \right) F_\tau u_\tau^k + \left((\boldsymbol{D}_{np}^k + \boldsymbol{D}_{nz}^k - \boldsymbol{A}_n^k)F_s \delta u_s^k \right)^T$$
$$\times \left(F_r \boldsymbol{Q}_{npr}^k (\boldsymbol{D}_p^k + \boldsymbol{A}_p^k) + F_r \boldsymbol{Q}_{nnr}^k (\boldsymbol{D}_{np}^k + \boldsymbol{D}_{nz}^k - \boldsymbol{A}_n^k) \right)$$
$$\times F_\tau u_\tau^k \right] d\Omega_k dz = \delta L_e^k - \delta L_{in}^k. \tag{46}$$

In Eq. (46), in order to obtain a strong form of differential equations on the domain Ω_k and the relative boundary conditions on edge Γ^k, the integration by parts is used, which permits to move the differential operator from the infinitesimal variation of the generic variable $\delta\boldsymbol{a}^k$ to the finite quantity $\boldsymbol{a}^k$ [28]. Only the static case is investigated in this work, so the virtual variation of the inertial forces δL_{in}^k is not in considered.

By considering the integration by parts, and the governing equation in the following form:

$$\delta u_s^k : \quad \boldsymbol{K}_{uu}^{k\tau sr} \boldsymbol{u}_\tau^k = \boldsymbol{p}_\tau^k, \tag{47}$$

with related boundary conditions on edge Γ_k:

$$\prod_{uu}^{k\tau sr} \boldsymbol{u}_\tau^k = \prod_{uu}^{k\tau sr} \bar{\boldsymbol{u}}_\tau^k, \tag{48}$$

(where $\boldsymbol{p}_{us}^k$ is the mechanical load and $\boldsymbol{u}_\tau^k$ is the vector of the degrees of freedom for the displacements) the fundamental nucleus $\boldsymbol{K}_{uu}^{k\tau sr}$ for the stiffness matrix and the fundamental nucleus $\prod_{uu}^{k\tau sr}$ for the uu uu boundary conditions are:

$$\boldsymbol{K}_{uu}^{k\tau sr} = \int_{A_k} \left[\left(-\boldsymbol{D}_p^k + \boldsymbol{A}_p^k \right)^T \left(F_r \boldsymbol{Q}_{ppr}^k (\boldsymbol{D}_p^k + \boldsymbol{A}_p^k) + F_r \boldsymbol{Q}_{pnr}^k \right. \right.$$
$$\times \left(\boldsymbol{D}_{np}^k + \boldsymbol{D}_{nz}^k - \boldsymbol{A}_n^k) \right) + \left(-\boldsymbol{D}_{np}^k + \boldsymbol{D}_{nz}^k - \boldsymbol{A}_n^k \right)^T$$
$$\times \left(F_r \boldsymbol{Q}_{npr}^k (\boldsymbol{D}_p^k + \boldsymbol{A}_p^k) + F_r \boldsymbol{Q}_{nnr}^k (\boldsymbol{D}_{np}^k + \boldsymbol{D}_{nz}^k - \boldsymbol{A}_n^k) \right) \right]$$
$$\times F_s F_\tau H_\alpha^k H_\beta^k dz, \tag{49}$$

$$\prod_{uu}^{k\tau sr} = \int_{A_k} \left[\boldsymbol{I}_p^{kT} \left(F_r \boldsymbol{Q}_{ppr}^k (\boldsymbol{D}_p^k + \boldsymbol{A}_p^k) + F_r \boldsymbol{Q}_{pnr}^k \right. \right.$$
$$\left. \times (\boldsymbol{D}_{np}^k + \boldsymbol{D}_{nz}^k - \boldsymbol{A}_n^k) \right) + \boldsymbol{I}_{nP}^{kT} \left(F_r \boldsymbol{Q}_{npr}^k (\boldsymbol{D}_p^k + \boldsymbol{A}_p^k) \right.$$
$$\left. \left. + F_r \boldsymbol{Q}_{nnr}^k (\boldsymbol{D}_{np}^k + \boldsymbol{D}_{nz}^k - \boldsymbol{A}_n^k) \right) \right] F_s F_\tau H_\alpha^k H_\beta^k dz. \quad (50)$$

$\boldsymbol{I}_p^k$ and $\boldsymbol{I}_{np}^k$ are identity matrices to perform the integration by parts. Details about fundamental nuclei *pnp* in Eqs. (49) and (50), in particular their algebraic closed form and the complete assembling procedure, can be found in [28].

5.2. Advanced Models

In the case of pure mechanical problems, Reissner's mixed variational theorem (RMVT) states as indicated:

$$\int_V \left(\delta \boldsymbol{\epsilon}_{pG}^T \boldsymbol{\sigma} pc + \delta \boldsymbol{\epsilon}_{nG}^T \boldsymbol{\sigma}_{nM} + \delta \boldsymbol{\sigma}_{nM}^T (\boldsymbol{\epsilon}_{nG} - \boldsymbol{\epsilon}_{nC}) \right) dV$$
$$= \delta L_e - \delta L_{in}. \quad (51)$$

The subscript *M* means a priori modelled variable. By considering a multilayered structure constituted by N_l layers, the Eq. (51) can be rewritten as:

$$\sum_{K=1}^{N_1} \int_{\Omega_k} \int_{A_k} \left\{ \delta \boldsymbol{\epsilon}_{pG}^T \boldsymbol{\sigma}_{pC}^k + \delta \boldsymbol{\epsilon}_{nG}^{k}{}^T \boldsymbol{\sigma}_{nM}^k + \delta \boldsymbol{\sigma}_{nM}^{k}{}^T \left(\boldsymbol{\epsilon}_{nG}^k - \boldsymbol{\epsilon}_{nC}^k \right) \right\}$$
$$\times d\Omega_k dz = \sum_{k=1}^{N_1} \delta L_e^k - \sum_{k=1}^{N_1} \delta L_{in}^k. \quad (52)$$

The relative constitutive equations for the RMVT case have been given in Eqs. (40) and (41). Substituting these equations in Eq. (52), by considering the geometrical relations of Section 2, and substituting CUF [24] as presented in Section 3; for a generic layer *k*:

$$\int_{\Omega_k} \int_{A_k} \left[\left((\boldsymbol{D}_p^k + \boldsymbol{A}_p^k) F_s \delta \boldsymbol{u}_s^k \right)^T \left(F_r \hat{\boldsymbol{Q}}_{ppr}^k (\boldsymbol{D}_p^k + \boldsymbol{A}_p^k) F_\tau \boldsymbol{u}_\tau^k \right. \right.$$
$$\left. + F_r \hat{\boldsymbol{Q}}_{pnr}^k F_\tau \boldsymbol{\sigma}_{nM\tau}^k \right) + \left((\boldsymbol{D}_{np}^k + \boldsymbol{D}_{nz}^k - \boldsymbol{A}_n^k) F_s \delta \boldsymbol{u}_s^k \right)^T$$
$$\times \left(F_\tau \boldsymbol{\sigma}_{nM\tau}^k \right)^T + (F_s \delta \boldsymbol{\sigma}_{nMs}^k)^T \left((\boldsymbol{D}_{np}^k + \boldsymbol{D}_{nz}^k - \boldsymbol{A}_n^k) F_\tau \boldsymbol{u}_\tau^k \right.$$
$$\left. \left. - F_r \hat{\boldsymbol{Q}}_{npr}^k (\boldsymbol{D}_p^k + \boldsymbol{A}_p^k) F_\tau \boldsymbol{u}_\tau^k - F_r \hat{\boldsymbol{Q}}_{nnr}^k F_T \boldsymbol{\sigma}_{nM\tau}^k \right) \right]$$
$$\times d\Omega_k d_z = \delta L_e^k - \delta L_{in}^k. \quad (53)$$

In Eq. (53), in order to obtain a strong form of differential equations on the domain Ω_k and the relative boundary conditions on edge Γ_k, the integration by parts is used [29]. The governing equations have the following form:

$$\delta \boldsymbol{u}_s^k: \quad \boldsymbol{K}_{uu}^{k\tau sr} \boldsymbol{u}_\tau^k + \boldsymbol{K}_{u\sigma}^{k\tau sr} \boldsymbol{\sigma}_{nM\tau}^k = \boldsymbol{p}_{us}^k, \quad (54)$$
$$\delta \boldsymbol{\sigma}_{nMs}^k: \quad \boldsymbol{K}_{\sigma u}^{k\tau sr} \boldsymbol{u}_r^k + \boldsymbol{K}_{\sigma\sigma}^{k\tau sr} \boldsymbol{\sigma}_{nM\tau}^k = 0. \quad (55)$$

Along with these governing equations the following boundary conditions on the edge γ_k of the in-plane integration domain Ω_k hold:

$$\prod_{uu}^{k\tau sr} \boldsymbol{u}_\tau^k + \prod_{u\sigma}^{k\tau sr} \boldsymbol{\sigma}_{nM\tau}^k = \prod_{uu}^{k\tau sr} \bar{\boldsymbol{u}}_\tau^{-k} + \prod_{u\sigma}^{k\tau sr} \bar{\boldsymbol{\sigma}}_{nM\tau}^{-k}$$
$$(56)$$

The fundamental nuclei can be obtained:

$$\boldsymbol{K}_{uu}^{k\tau sr} = \int_{A_k} \left[(-\boldsymbol{D}_p^k + \boldsymbol{A}_p^k) T \left(F_r \hat{\boldsymbol{Q}}_{ppr}^k (\boldsymbol{D}_p^k + \boldsymbol{A}_p^k) \right) \right]$$
$$\times F_s F_\tau H_\alpha^k H_\beta^k dz, \quad (57)$$

$$\boldsymbol{K}_{u\sigma}^{k\tau sr} = \int_{A_k} \left[(-\boldsymbol{D}_p^k + \boldsymbol{A}_p^k)^T \left(F_r \hat{\boldsymbol{Q}}_{pnr}^k \right) \right.$$
$$\left. \times (-\boldsymbol{D}_{np}^k + \boldsymbol{D}_{nz}^k - \boldsymbol{A}_n^k) \right] F_s F_\tau H_\alpha^k H_\beta^k dz, \quad (58)$$

$$\boldsymbol{K}_{\sigma u}^{k\tau sr} = \int_{A_k} \left[(\boldsymbol{D}_{np}^k + \boldsymbol{D}_{nz}^k - \boldsymbol{A}_n^k) - \left(F_r \hat{\boldsymbol{Q}}_{pnr}^k \right) \right.$$
$$\left. \times (\boldsymbol{D}_p^k + \boldsymbol{A}_p^k) \right] F_s F_r H_\alpha^k H_\beta^k dz, \quad (59)$$

$$\boldsymbol{K}_{\sigma\sigma}^{k\tau sr} = \int_{A_k} \left[- F_r \hat{\boldsymbol{Q}}_{nnr}^k \right] F_s F_\tau H_\alpha^k H_\beta^k dz, \quad (60)$$

The nuclei for boundary conditions on edge γ_k are:

$$\prod_{uu}^{k\tau sr} = \int_{A_k} \left[\boldsymbol{I}_p^{kT} F_r \hat{\boldsymbol{Q}}_{ppr}^k (\boldsymbol{D}_p^k + \boldsymbol{A}_p^k) \right] F_s F_r H_\alpha^k H_\beta^k dz, \quad (61)$$

$$\prod_{u\sigma}^{k\tau sr} = \int_{A_k} \left[\boldsymbol{I}_p^{kT} F_r \hat{\boldsymbol{Q}}_{pnr}^k + \boldsymbol{I}_{np}^{kT} \right] F_s F_r H_\alpha^k H_\beta^k dz. \quad (62)$$

Algebraic closed form of nuclei in Eqs. (57)–(60) and in Eqs. (61) and (62) are detailed in [29].

5.3. Closed Form Solution

Developing the matrices products in Eqs. (49) and (50), fundamental nuclei of dimension [3 × 3] in differential form are obtained for the PVD case. For the RMVT case, the differential form of the [3 × 3] fundamental nuclei are obtained by developing the matrice products in Eqs. (57)–(60) and in Eqs. (61) and (62).

Navier-type closed-form solutions are obtained via substitution of harmonic expressions for the displacements and transverse stresses, as well as by considering the following material coeffcients to be equal to zero: $Q_{16r} = Q_{26r} = Q_{36r} = Q_{45r} = 0$. The following harmonic assumptions can be made for the variables, which correspond to simply supported boundary

conditions:

$$\left(u_\tau^k, \sigma_{\alpha z\tau}^k\right) = \sum_{m,n} \left(\hat{U}_\tau^k, \hat{\sigma}_{\alpha z\tau}^k\right) \cos\left(\frac{m\pi\alpha_k}{\alpha_k}\right) \sin\left(\frac{n\pi\beta_k}{b_k}\right),$$
$$k = 1, N_l \tag{63}$$

$$\left(u_\tau^k, \sigma_{\beta z\tau}^k\right) = \sum_{m,n} \left(\hat{V}_\tau^k, \hat{\sigma}_{\beta z\tau}^k\right) \sin\left(\frac{m\pi\alpha_k}{\alpha_k}\right) \cos\left(\frac{n\pi\beta_k}{b_k}\right),$$
$$\tau = t, b, \Gamma \tag{64}$$

$$\left(w_\tau^k, \sigma_{zz\tau}^k\right) = \sum_{m,n} \left(\hat{W}_\tau^k, \hat{\sigma}_{zz\tau}^k\right) \sin\left(\frac{m\pi\alpha_k}{\alpha_k}\right) \sin\left(\frac{n\pi\beta_k}{b_k}\right),$$
$$\tau = 2, N \tag{65}$$

where $\hat{U}_\tau^k$, $\hat{V}_\tau^k$, $\hat{W}_\tau^k$ are the displacement amplitudes, and $\hat{\sigma}_{\alpha z\tau}^k$, $\hat{\sigma}_{\beta z\tau}^k$, $\hat{\sigma}_{zz\tau}^k$ are the transverse shear/normal stress amplitudes. m and and n are the in-plane wave numbers in the α and β directions, a and b are the in-plane plate/shell dimensions, k is indicative of the layer and Nl is the total number of layers.

The closed algebraic forms of the fundamental nuclei are given in detail in [28] for the PVD case and in [29] for the RMVT case.

5.4. Assembling Procedure

By starting from a [3 × 3] fundamental nucleus, the matrix of the considered multilayer is obtained by expanding via the index r in the case of FGM layers (see Section 4), via the indexes τ and s for the order of expansion in the thickness direction (see Section 3) and via the index k for the multilayer assembling (equivalent single layer [ESL] or Layer Wise [LW]). Examples of assembling procedures for a three layered structure with the internal core in FGM are given in Figures 4 and 5. If there are no FGM layers, the assembling on index r is not considered [28, 29]. The ESL and LW assembling procedures are described in Figure 4. Transverse shear and normal stresses are always considered in the LW form, therefore the ESL procedures for nuclei $\boldsymbol{K}_{u\sigma}$ and $\boldsymbol{K}_{\sigma u}$ are those given in Figure 5.

5.5. Acronyms

CUF permits several hierarchical two-dimensional models to be obtained, therefore a system of acronyms has been developed to indicate such theories. The letter E or L is employed if the multilayer assembling is in ESL or LW form, respectively. D indicates displacement formulation based on PVD and M indicates advanced/mixed models based on RMVT. A number from 1 to 4 is added to indicate the order of expansion in the thickness direction z (from linear to fourth order). Therefore, ED1-ED4
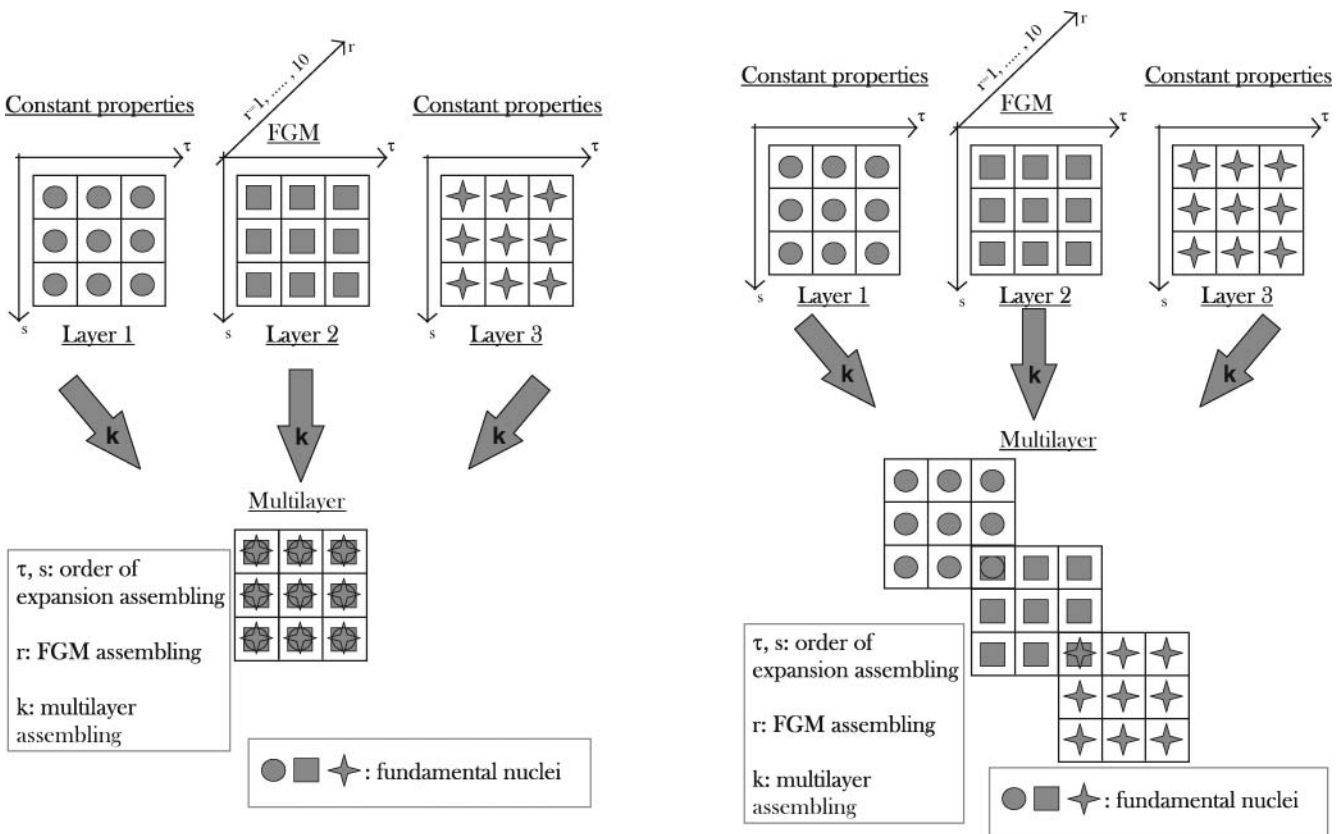

FIG. 4. Three-layered structure with the internal core in FGM. ESL (left) and LW (right) assembling procedures.
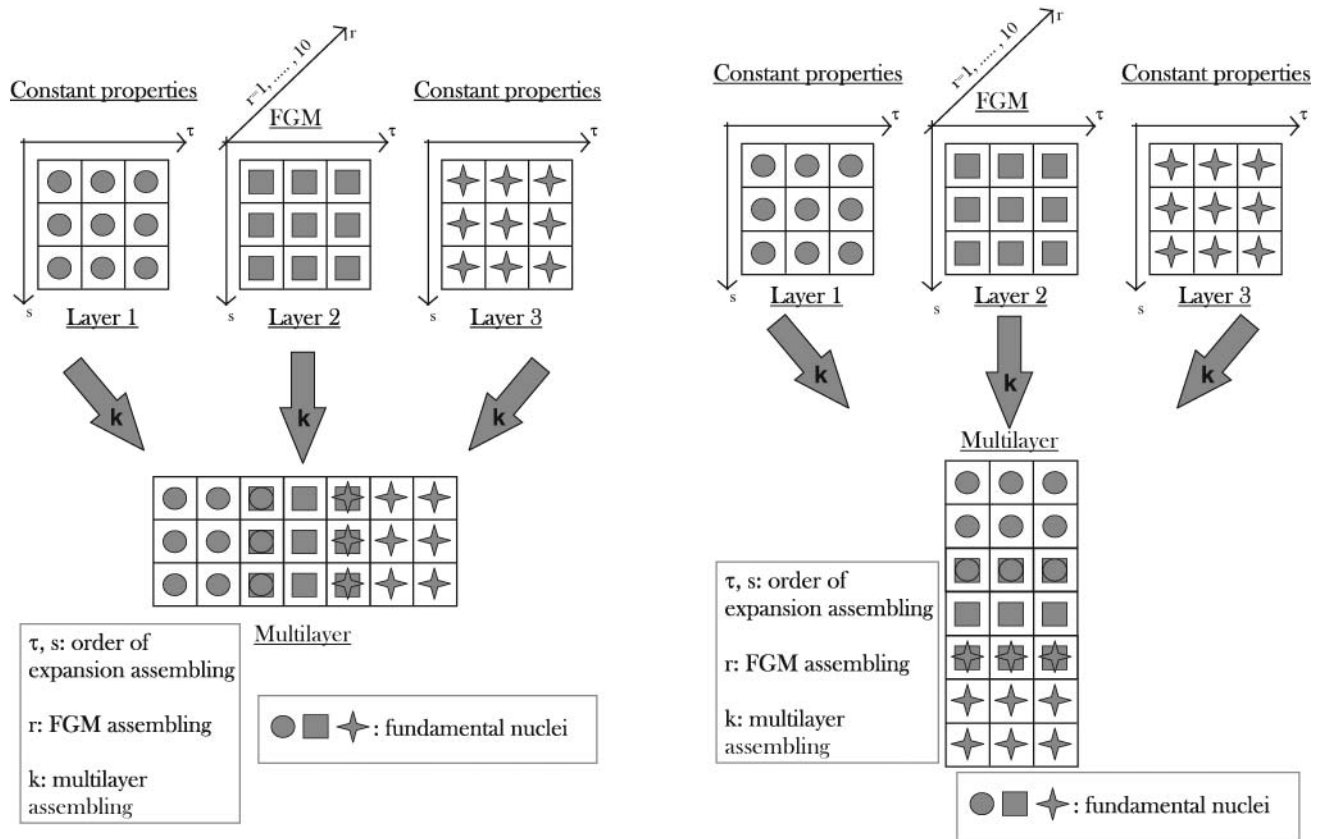
FIG. 5.   Three-layered structure with the internal core in FGM. ESL assembling procedure for $K_{u\sigma}$ (left) and ESL assembling procedure for $K_{\sigma u}$ (right).

and LD1-LD4 are the refined models (PVD) in the ESL and LW approaches, respectively. EM1-EM4 and LM1-LM4 are the corresponding mixed models based on RMVT. A further letter Z is added in the ESL theories when MZZF is introduced in order to obtain the typical ZZ form of displacements; these theories are indicated as EDZ1-EDZ3 and EMZ1-EMZ3. The First order Shear Deformation Theory (FSDT) is obtained from the ED1 model by considering a constant transverse displacement w in the z direction, the Classical Lamination Theory (CLT) also considers an infinite shear rigidity.

6.   RESULTS

The bending response of several multilayered plates and shells embedding FGM layers is here investigated. First, two preliminary assessments for plate and shell geometries are given in order to validate the proposed refined and advanced two-dimensional models as quasi-3D solutions. In the second part, the effects of several FGM configurations, in multilayered plates and shells, are investigated by means of the advanced LM4 theory. The effects of κ (exponent for the FGM law) and h_{FGM} (thickness of the FGM layers) are also considered.

6.1.   Preliminary Assessments

The first assessment considers a sandwich plate with a functionally graded core. The structure is simply supported with

a bi-sinusoidal ($m = n = 1$) load applied at the top in the z direction, the amplitude is $\bar{p}_z = 1\,Pa$. The plate is square ($a = b = 3$ m) with a thickness ratio of $a/h_0 = 3$. The exact three-dimensional solution is given by Kashtalyan and Menshykova [9]. The geometry of the plate is clearly indicated in Figure 6, the global thickness of the plate is $h_0 = 2h$, where h and $-h$ are the top and bottom coordinates of the plate, respectively and h_c and $-h_c$ are the coordinates of the bottom 4th layer and the top 1st layer, respectively. The global thickness of the core is $2h_c$. The plate has a global thickness $h_0 = 1.0$ m, while the thickness of the two faces is $h_f = 0.1h_0$, and the thickness of the core is $2h_c = 0.8h_0$. The Young modulus of reference is $E_0 = 73$ GPa with a Poisson ratio $\nu = 0.3$, and the two faces consequently have a constant shear modulus $G_f = G_0 = 28.08$ GPa (layers 1 and 4). The core can be divided into parts 2 and 3. The value of the shear modulus in the middle reference surface is indicated with Gc. In layer 2, the exponential law for the shear modulus is $G(z) = G_0 e^{[-\gamma(z/h_c+1)]}$ with $h_c = 0.4$ m and $-0.4 \le z \le 0$. For layer 3, the exponential law is $G(z) = G_0 e^{[\gamma(z/h_c-1)]}$ with $h_c = 0.4$ m and $0 \le z \le 0.4$. Three different cases that correspond to three different shear modulus ratios G_c/G_f (0.9, 0.999, 1.0), which means values of the exponent γ equal to 0.105360, 0.001000 and 0.0, respectively, are considered. The $Gc/G_f = 1.0$ case means a three layered plate embedding the same material with constant
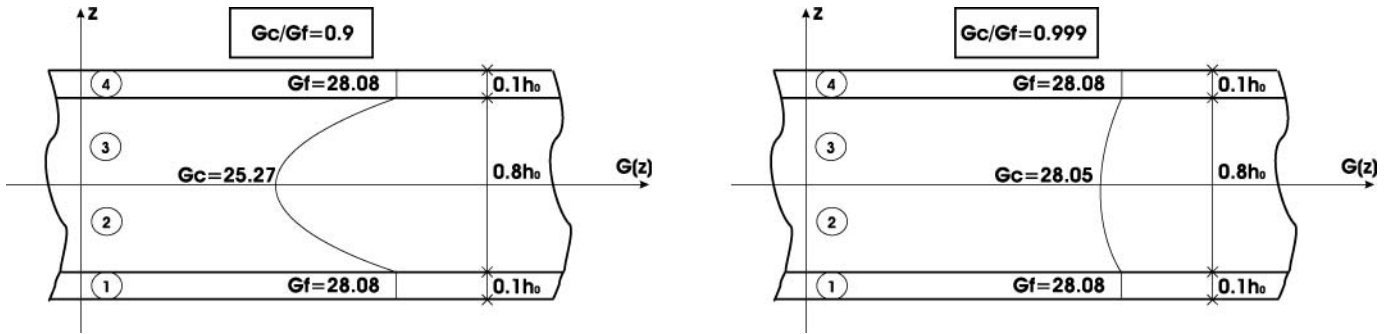
FIG. 6.   First assessment, sandwich plate with an FGM core. Core-face shear modulus ratio G_c/G_f equals 0.9 on the left and 0.999 on the right.

elastic properties in the thickness direction. A comparison between the three-dimensional solution [9] and classical, refined and advanced two-dimensional models is proposed in Table 1 for the no-dimensional transverse displacement $\bar{w}$ in the middle of the plate. The 3D solution is obtained for each value of the shear modulus ratio Gc/G_f, by means of layer wise models and higher orders of expansion in the thickness direction z (LD4 and LM4 theories). Classical models, such as CLT and FSDT, give a larger error. Table 2 proposes the transverse normal stress σ_{zz} at the top of the sandwich plate; the reference solution is given by the boundary loading conditions (a transverse normal mechanical load applied at the top equals 1.0 Pa). The LD4 and LM4 models achieve the three-dimensional result for each value of G_c/G_f. The use of advanced models improves the 3D-convergence speed of layer-wise theories, as clearly indicated by a comparison of the LD2 and LM2 models in Table 2. Figure 7, for the shear modulus ratio $G_c/G_f = 0.9$, gives the transverse displacement $\bar{w}$, the in-plane stress σ_{xy}, the transverse shear stress σ_{xz} and the transverse normal stress σ_{zz} through the thickness direction z. The correct evaluation in z is obtained by means of layer-wise theories and higher orders of expansion.

The second assessment considers a cylindrical shell panel with a radius of curvature in the β direction $R_\beta = \infty$ and radius of curvature in the α direction $R_\alpha = 10$ m. The angle Φ equals π/3, therefore the two dimensions of the panel are $a = \pi/3 \ R_\alpha$ and $b = 1$ m. The shell is simply supported with a bisinusoidal mechanical load ($m = n = 1$) applied at the top ($\bar{p}_z = 1 \ Pa$). First, only an FGM layer is considered where the Young modulus changes according to Zenkour [15] with a polynomial law $E(z) = E_m + (E_c - E_m)(\frac{2z+h}{2h})^\kappa$ where $-\frac{h}{2} \le z \le \frac{h}{2}$. The FGM is fully metallic at the bottom, where $E_m = 70$ GPa and fully ceramic at the top, where $E_c = 380$ GPa; the Poisson ratio is considered constant and equal to 0.3, and the exponent κ varies from 1 to 10. In order to test our refined and advanced models, a quasi-3D reference solution (Ref) for the FGMs was developed in [28] and [29] employing a layer-wise model with fourth-order of expansion in the thickness direction and by dividing the FGM layer into 100 mathematical layers with constant properties: the method is computationally very expensive, but it is incisive. Then, a sandwich shell with an FGM core is investigated, the bottom face is in metallic material with the Young modulus $E_m = 70$ GPa and the top face is in ceramic

TABLE 1
First assessment, sandwich plate with an FGM core.
No-dimensional transverse displacement $\bar{w} = w \frac{G_0}{\bar{p}_z h_0}$ in the middle of the plate

$\frac{Gc}{G_f}$	$\bar{w}(z = 0)$		
	0.9	0.999	1.0
3D[9]	1.4227	1.3433	1.3430
LM4	1.4227	1.3432	1.3426
LM3	1.4228	1.3435	1.3428
LD4	1.4227	1.3432	1.3426
LD3	1.4227	1.3432	1.3425
ED4	1.4199	1.3432	1.3424
ED2	1.3067	1.2792	1.2789
FSDT	1.1924	1.1690	1.1687
CLT	1.3513	1.3295	1.3292

TABLE 2
First assessment, sandwich plate with an FGM core.
Transverse normal stress σ_{zz} at the top of the plate. L.C. means boundary loading conditions

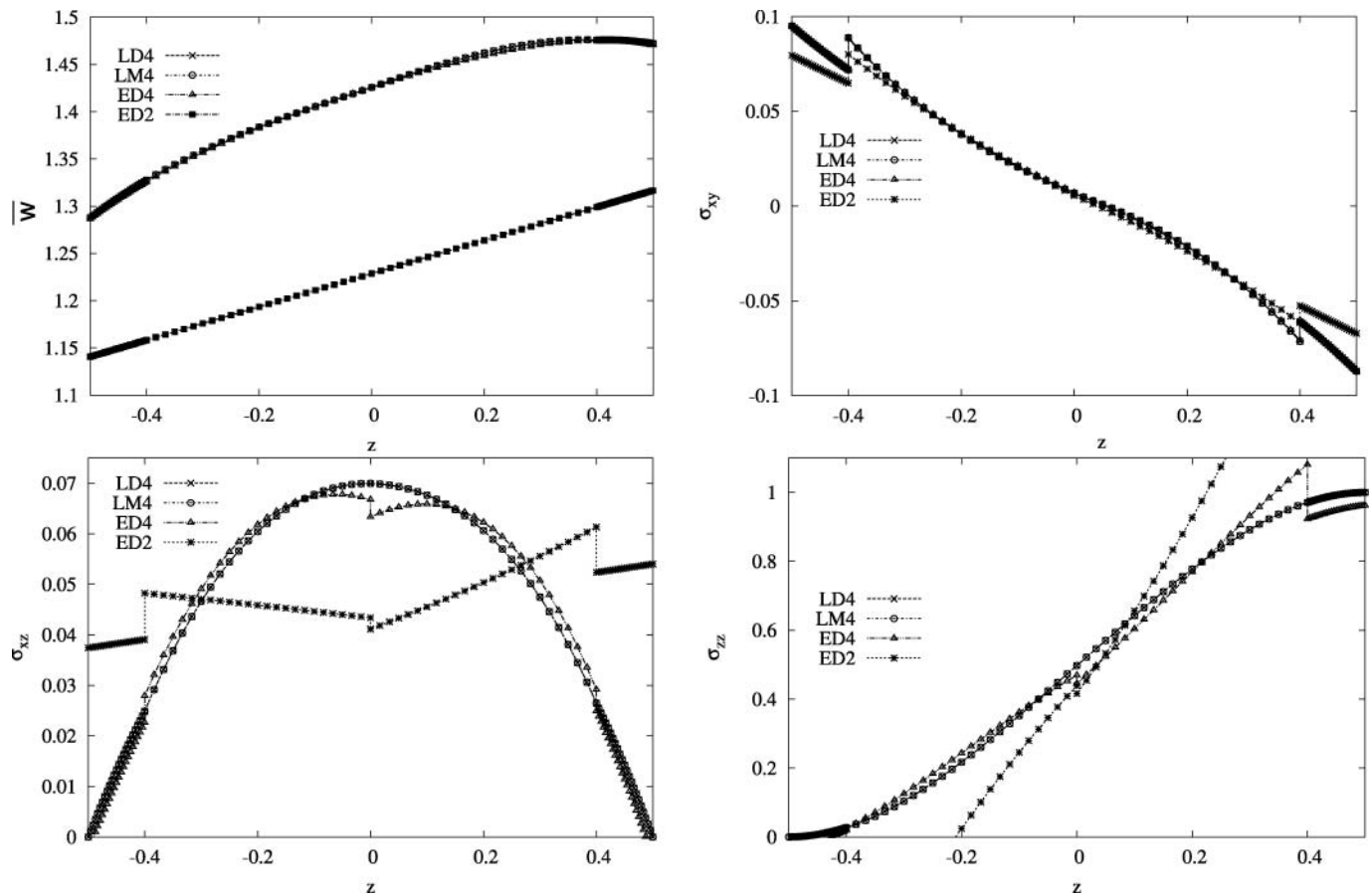| $\frac{Gc}{G_f}$	$\sigma_{zz}(z = h)$		
	0.9	0.999	1.0
L.C.	1.0000	1.0000	1.0000
LM4	1.0000	1.0000	1.0000
LM2	1.0046	1.0067	1.0066
LD4	1.0000	1.0000	1.0000
LD2	1.0119	1.0119	1.0119
ED4	0.9060	1.0026	1.0035
ED3	1.1766	1.2226	1.2271
FSDT	1.1536	1.1723	1.1724
CLT	2.0013	1.9845	1.9842

FIG. 7.   First assessment, sandwich plate with an FGM core. Displacement and stresses through the thickness z for Gc/G_f equals 0.9.

material with $E_c = 380$ GPa. The core consists of an FGM with the Young modulus varying in z, according to Zenkour's formula [15] (the same material as the one-layered case). The thickness of each face is $h_f = 0.1h$ and the core has $h_c = 0.8$ h. In the core, the Young modulus $E(z)$ changes in z according to several values of the exponent κ. A reference solution (Ref) has been provided with the same method described for the one-layered case (for details see [28] and [29]). The transverse displacement $\bar{w}$, for several thickness ratios R_α/h and exponents κ, is given in Table 3 for the one-layered FGM shell; the use of refined models with higher orders of expansion permits a quasi-3D evaluation of the static response of functionally graded shells. An FGM sandwich configuration is proposed in Table 4 where the three-dimensional value of the transverse normal stress at the top is given by the boundary loading conditions; this value is correctly achieved by the LM4 model for each value of the thickness ratio R_α/h and exponent κ.

The two proposed assessments demonstrate that the LM4 model gives a quasi-3D response, in terms of displacements and stresses, of one-layered and multilayered plates and shells embedding FGM layers. In the next section, the LM4 model is used to investigate the effects of introducing some FGM layers into common sandwich plates and shells.

6.2.   Multilayered FGM Plates and Shells

The considered sandwich plate is simply supported with a bi-sinusoidal ($m = n = 1$) load of amplitude $\bar{p}_z = 1$ Pa applied at the top. The plate is square ($a = b = 1$ m) with a total thickness $h = 0.02$ m, therefore the thickness ratio is $a/h = 50$. Each external face has a thickness $h_f = 0.1$ h; the top face is in ceramic material with Young modulus $E_c = 380$ GPa and Poisson ratio $\nu = 0.3$, the bottom face is in metallic material with $E_m = 70$ GPa and $\nu = 0.3$. The core has a thickness $h_c = 0.8$ h and several configurations are employed in order to investigate the effects of the introduction of FGM layers. The possible configurations are clearly shown in Figure 8: a core in Nomex with Young modulus $E = 1$ MPa and Poisson ratio $\nu = 0.3$ is employed first, then two functionally graded inter-layers are introduced between the top ceramic face and the Nomex core, and the bottom metallic face and the Nomex core. The Young modulus changes according to Zenkour's law [15], which has already been given in Section 6.1; according to this law, several values of the exponent κ can be employed from $E_c = 380$ GPa to $E = 1$ MPa at the top, and from $E_m = 70$ GPa to $E = 1$ MPa at the bottom. A parameter $q = \frac{h_{FGM}}{h_{core}}$ is given to define the thickness of the employed FGM inter-layers; when $q = 1$, the core is completely in FGM and the Young modulus
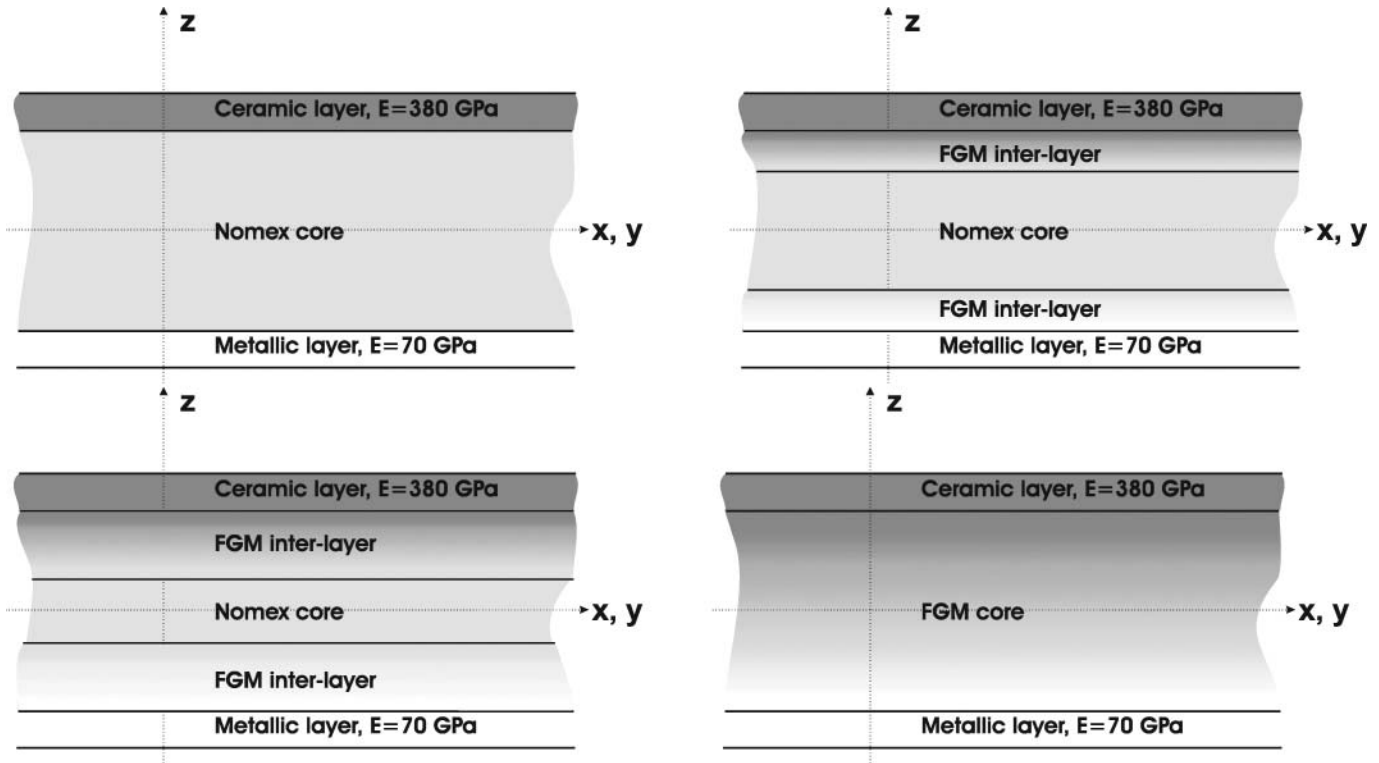
FIG. 8.   Several configurations of sandwich plate: core in Nomex, core in Nomex with two FGM inter-layers ($h_{FGM}/h_{core} = 0.5$ and $h_{FGM}/h_{core} = 0.75$), core in FGM.

TABLE 3
Second assessment, one-layered FGM cylindrical shell.
Transverse displacement $\bar{w} = w \times 10^{10}$ in the middle of the shell

		$\bar{w}(z = 0)$			
	R_α/h	4	10	100	1000
$\kappa = 1$	Ref	0.0018	0.0170	52.781	4201.3
	LM4	0.0013	0.0170	52.783	4201.4
	LD4	0.0013	0.0170	52.783	4201.4
	LM2	0.0013	0.0162	52.693	4201.4
	LD2	0.0014	0.0162	52.692	4201.4
	FSDT	0.0054	0.0170	43.735	3792.2
$\kappa = 4$	Ref	0.0032	0.0314	79.739	7081.1
	LM4	0.0022	0.0315	79.734	7081.6
	LD4	0.0021	0.0315	79.734	7081.6
	LM2	0.0028	0.0287	79.345	7081.6
	LD2	0.0032	0.0288	79.344	7081.6
	FSDT	0.0090	0.0277	65.603	6384.2
$\kappa = 10$	Ref	0.0042	0.0404	92.018	9370.8
	LM4	0.0022	0.0405	92.033	9373.1
	LD4	0.0021	0.0404	92.014	9373.1
	LM2	0.0044	0.0359	91.356	9373.0
	LD2	0.0049	0.0355	91.304	9373.0
	FSDT	0.0121	0.0358	75.561	8436.5

changes with continuity from the bottom ($E_m = 70$ GPa) to the top ($E_c = 380$ GPa). When $q = 0$, the core is completely in Nomex and no FGM inter-layers are embedded in the structure. Table 5 gives the maximum value in the z direction for the transverse displacement w, the in-plane stress σ_{xx} and the transverse shear stress σ_{xz}. The investigated cases are: core completely in Nomex ($q = 0$), core completely in FGM ($q = 1$), and several thicknesses of FGM inter-layers embedded between the two faces and the core in Nomex ($q = 0.25, 0.5, 0.75$). When the FGM inter-layers are used, several exponents of Zenkour's law are investigated ($\kappa = 1, 5, 10$). The use of the core in Nomex gives the largest values for the displacements and the stresses, while the smallest values are shown when the core is completely in FGM. The use of a complete FGM core leads to some problems, such as higher costs and higher weights, therefore several halfway configurations also have been investigated: if the thickness of the FGM inter-layers increases, the maximum values of displacements and stresses decrease. The displacements, in-plane stresses and transverse stresses for the sandwich with the core in Nomex are given in Figure 9. The displacements have the typical ZZ form of classical sandwich plates. This property is clearly given for the displacement u, and underlined for the displacement w in Figure 10, since it is not clearly shown in Figure 9 due to scale problems. The in-plane stresses are discontinuous at the interfaces between the faces and the core. The transverse stresses are continuous because
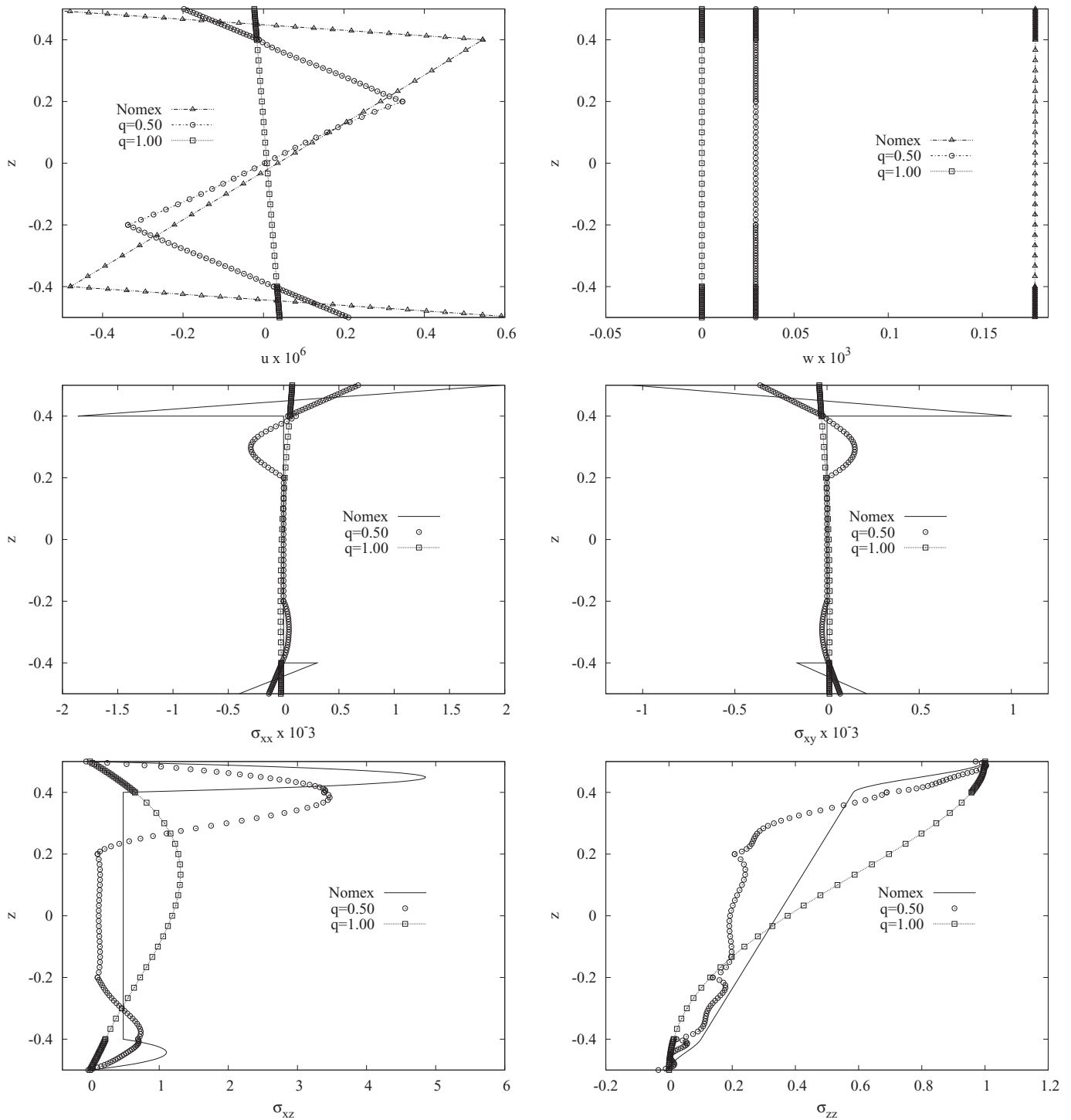
FIG. 9.   Sandwich plate with core in Nomex and/or FGM. Displacements, in-plane stresses and transverse stresses through the thickness z ($\kappa = 1$).

an LM4 theory is employed; transverse shear stress σ_{xz} has non-symmetric behavior since the sandwich is asymmetric (the two faces are different). Using an exponent $\kappa = 1$, the effect of the FGM inter-layers ($q = 0.5$) and core fully in FGM ($q = 1.0$) is also investigated in Figure 9: the maximum value of the

displacements and in-plane stresses is reduced and the typical ZZ effect is damped; the in-plane stresses are now continuous at the interfaces and the transverse stresses are reduced. Another important parameter is the employed exponent κ in the FGM law, shown in Figure 11 for $q = 0.25$ (left side) and $q = 0.75$

TABLE 4
Second assessment, sandwich cylindrical shell with core in
FGM. Transverse normal stress σ_{zz} at the top of the shell. L.C.
means boundary loading conditions

		$\sigma_{zz}(z = h/2)$			
	R_α/h	4	10	100	1000
$\kappa = 1$	L.C.	1.0000	1.0000	1.0000	1.0000
	LM4	1.0000	1.0000	1.0000	1.0000
	LD4	1.0009	1.0000	1.0000	1.0000
	LD2	1.0765	1.0257	1.0124	1.0000
	EM4	1.4163	1.0952	0.9675	0.9756
	ED4	1.4204	1.0959	0.9674	0.9756
	ED2	1.0733	1.2953	1.1173	0.8956
	EMZ3	2.0956	1.4603	1.2973	1.1088
	FSDT	0.0797	0.4464	42.278	776.77
$\kappa = 5$	L.C.	1.0000	1.0000	1.0000	1.0000
	LM4	1.0000	1.0000	1.0000	1.0000
	LD4	1.0010	1.0000	1.0000	1.0000
	LD2	1.0845	1.0307	1.0138	0.9998
	EM4	1.2988	0.8036	0.6404	0.8164
	ED4	1.3011	0.7977	0.6332	0.8159
	ED2	1.2457	1.5951	1.3997	0.9338
	EMZ3	2.7617	1.5077	1.3505	1.0326
	FSDT	0.0934	0.5155	49.864	1149.6
$\kappa = 10$	L.C.	1.0000	1.0000	1.0000	1.0000
	LM4	1.0000	1.0000	1.0000	1.0000
	LD4	1.0010	1.0000	1.0000	1.0000
	LD2	1.0856	1.0298	1.0147	0.9998
	EM4	1.2027	0.5142	0.3908	0.5989
	ED4	1.2179	0.5140	0.3883	0.6029
	ED2	1.3376	1.7534	1.5234	1.0486
	EMZ3	3.1867	1.6443	1.4872	1.0481
	FSDT	0.0987	0.5417	52.575	1320.4

FIG. 10.   Sandwich plate with core in Nomex, ZZ from of the transverse
displacement w.

TABLE 5
Sandwich plate, maximum values of displacement and stresses
in the thickness direction z for several values of the thickness
of the FGM inter-layers

$q = \frac{h_{FGM}}{h_{core}}$	k	w_{max}	$\sigma_{xx,max}$	$\sigma_{xz,max}$
0 (Nomex)		0.1782×10^{-3}	0.1959×10^4	4.8534
0.25	1	0.7162×10^{-4}	0.1201×10^4	4.5563
	5	0.1013×10^{-3}	0.1316×10^4	3.8106
	10	0.1097×10^{-3}	0.1317×10^4	3.5277
0.50	1	0.2968×10^{-4}	0.6478×10^3	3.4667
	5	0.5201×10^{-4}	0.7959×10^3	2.7398
	10	0.5950×10^{-4}	0.7667×10^3	2.3350
0.75	1	0.1422×10^{-4}	0.4033×10^3	2.3499
	5	0.2703×10^{-4}	0.4858×10^3	1.9541
	10	0.3239×10^{-4}	0.2807×10^4	2.2299
1	1	0.9999×10^{-6}	0.7804×10^2	1.3090
	5	0.1300×10^{-5}	0.8876×10^2	1.2146
	10	0.1331×10^{-5}	0.9289×10^2	1.1661

(right side) where three different values of κ are investigated. It
is clearly indicated how low values of κ reduce the transverse
stresses near the bottom of the plate and increase them near
the top. On the contrary, high values of κ increase the stresses
near the bottom and reduce them near the top. The exponent
$\kappa = 10$ is inappropriate for the reduction of in-plane stresses;
$\kappa = 1$ gives the continuity of in-plane stresses. The use of FGM
inter-layers is beneficial, but appropriate values of the thickness
(h_{FGM}) and opportune FGM laws (exponent κ) must be
employed.

TABLE 6
Sandwich shell, maximum values of displacement and stresses
in the thickness direction z for several values of the thickness
of the FGM inter-layers.

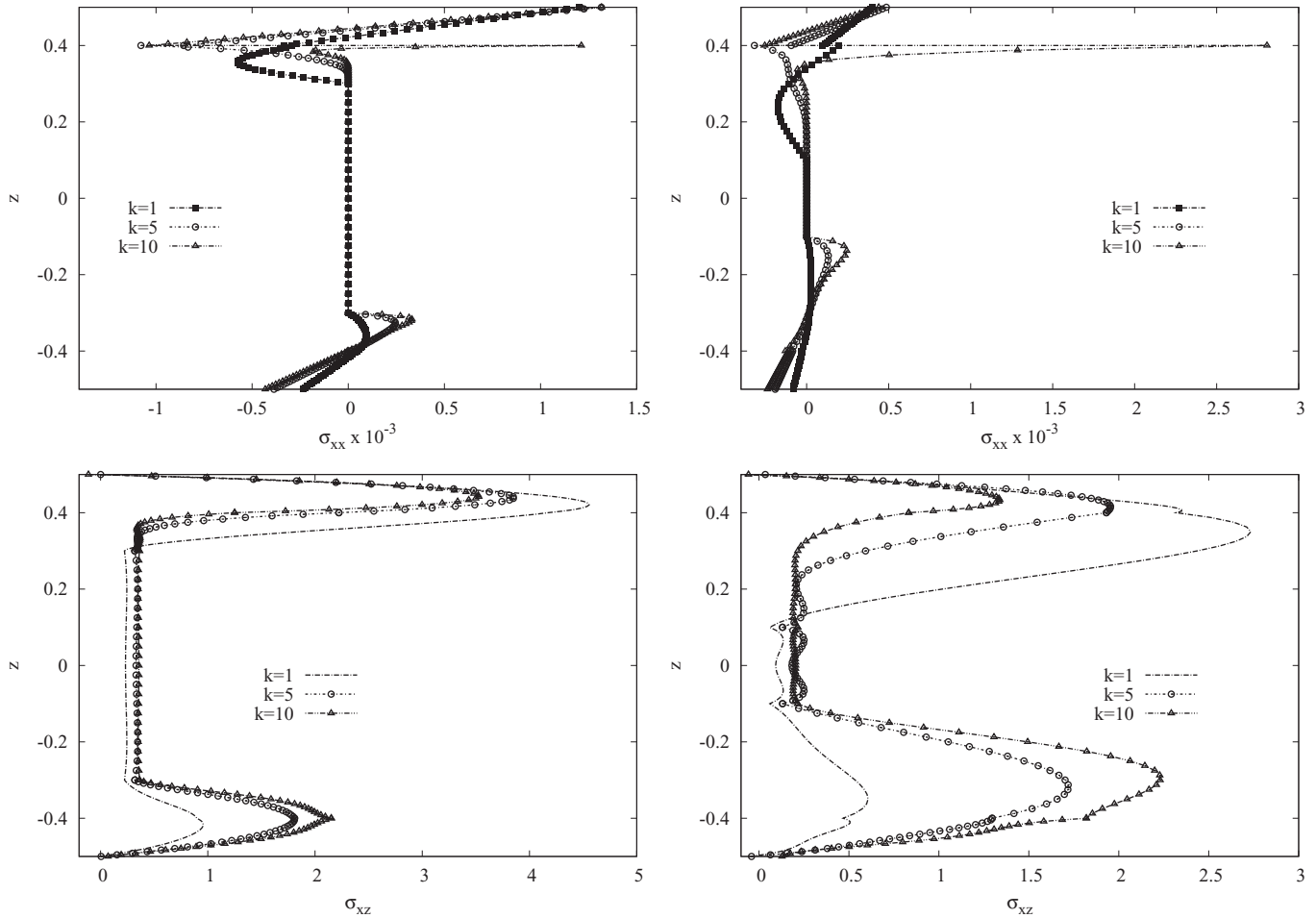| $q = \frac{h_{FGM}}{h_{core}}$	k	w_{max}	$\sigma_{\alpha\alpha,max}$	$\sigma_{\alpha z,max}$
0 (Nomex)		0.1845	0.5690×10^2	0.0307
0.25	1	0.1202	0.3848×10^2	0.0350
	3	0.1458	0.4581×10^2	0.0344
	10	0.1694	0.5239×10^2	0.0304
0.50	1	0.0894	0.2993×10^2	0.0351
	3	0.1234	0.3860×10^2	0.0333
	10	0.1591	0.4928×10^2	0.0301
0.75	1	0.0808	0.2558×10^2	0.0516
	3	0.1079	0.3384×10^2	0.0338
	10	0.1528	0.4737×10^2	0.0302
1	1	0.0220	0.8622×10^1	0.1698
	3	0.0301	0.1134×10^2	0.1628
	10	0.0379	0.1404×10^2	0.1708

FIG. 11.   Sandwich plate with core in Nomex and FGM inter-layers. Comparison for several values of the exponent κ. Fraction of the FGM thickness: $q = 0.25$ on the left and $q = 0.75$ on the right.

The second case considers a cylindrical shell panel with the same geometry given in the previous section: $R_\alpha = 10$ m, $R_\beta = \infty$, $a = \pi/3 \ R_\alpha$, $b = 1$ m. The shell is simply supported with a bi-sinusoidal ($m = n = 1$) load of amplitude $\bar{p}_z = 1 \ Pa$ applied at the top. The total thickness of the sandwich is $h = 0.2$ m, therefore the thickness ratio is $R\alpha/h = 50$. The sandwich configurations are the same as those given for the plate case: two external ceramic and metallic faces with the core either in Nomex, in FGM or in Nomex with inter-layers in FGMs. The employed FGM law for the Young modulus $E(z)$ is the same as that described in Zenkour's law [15]. The conclusions already drawn for the plate geometry also are confirmed for the shell configuration: the introduction of curvatures does not modify the beneficial effects obtained from the use of FGM inter-layers. Table 6 confirms, for several exponent values ($\kappa = 1, 3, 10$), that the introduction of FGM inter-layers reduces the maximum values of displacements and in-plane stresses, but this is not confirmed for the transverse stresses as in the plate

case. Obviously, the best configuration is the core completely in FGM. The displacements, in-plane stresses and transverse stresses in Figure 12 are given through the thickness direction z for a value of the exponent $\kappa = 3$; a comparison is made for the core in Nomex, FGM inter-layers ($q = 0.25$) and the core completely in FGM. Displacements are reduced by means of the FGM inter-layers and their ZZ forms are damped; the continuity of the in-plane stresses is guaranteed if FGM inter-layers are embedded in the structure. The exponent $\kappa = 3$ is not useful to reduce the maximum value of the in-plane stresses. When using the FGM inter-layers, the transverse stresses are better distributed in the thickness direction z. Figure 13 gives two different configurations of FGM inter-layers embedded between the Nomex core and the faces ($q = 0.5$ on the left and $q = 0.75$ on the right): the use of low values of κ is necessary to reduce or eliminate the in-plane stress discontinuity at the interfaces. On the contrary, the use of high values of κ is mandatory to reduce the maximum value of the transverse stress near the top.
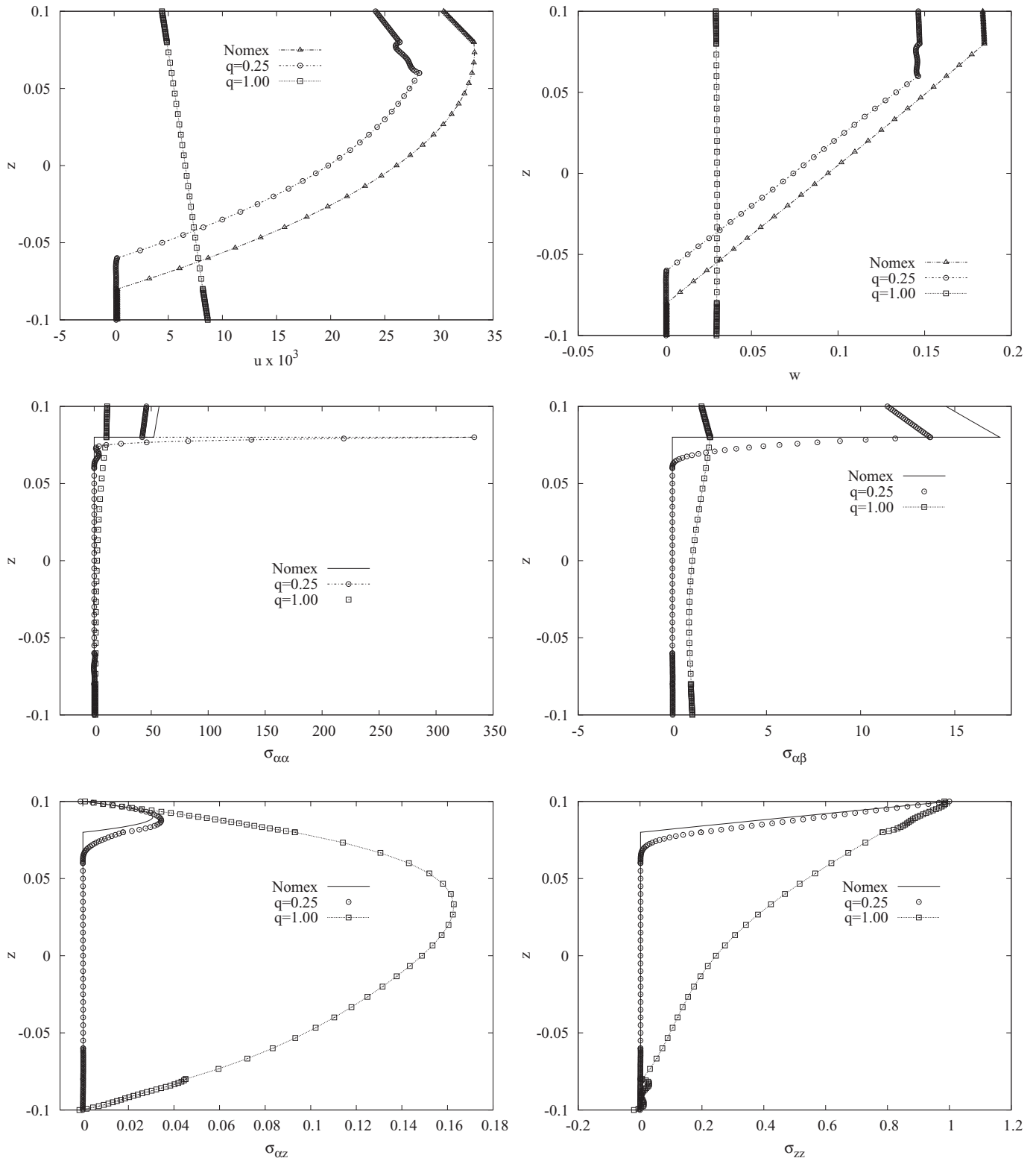
FIG. 12.   Sandwich shell with core in Nomex and/or FGM. Displacements, in-plane stresses and transverse stresses though the thickness z ($k = 3$).
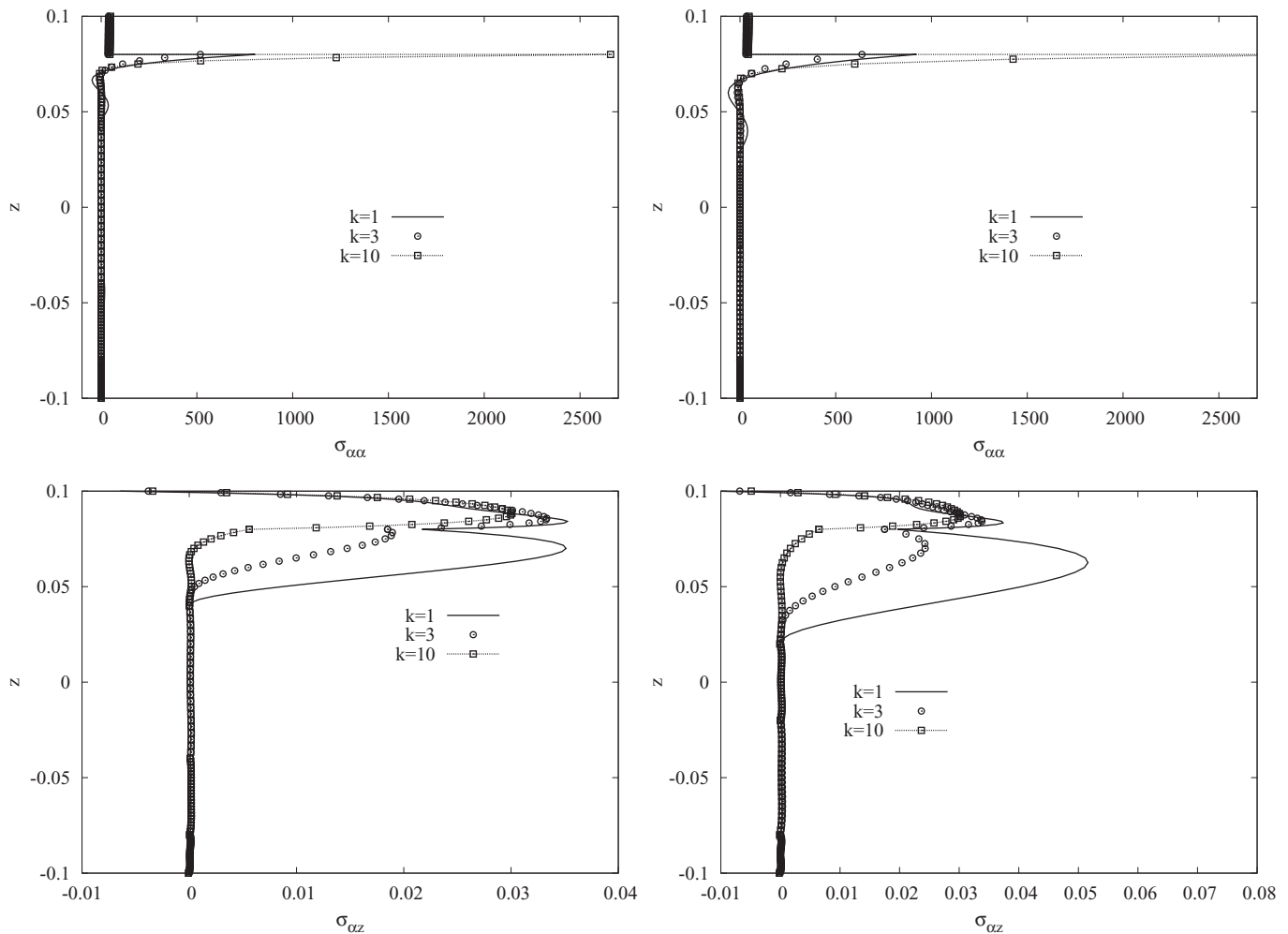
FIG. 13.   Sandwich shell with core in Nomex and FGM inter-layers. Comparison for several values of the exponent k. Fraction of the FGM thickness: $q = 0.5$ on the left and $q = 0.75$ on the right.

7.   CONCLUSIONS

The present paper has investigated the static response of several multilayered FGM plates and shells. First, the advanced layer-wise theory LM4 has been validated as a quasi-3D solution in the analysis of such structures. Sandwich plates and shells have been investigated using this model, in terms of displacements and stresses. The sandwich structures have two external faces in ceramic and metallic material at the top and bottom, respectively; the core is in Nomex. New configurations also consider the core totally in FGM, or with two FGM inter-layers embedded between the Nomex core and the two external faces. The use of FGMs leads to an improvement in the response of such sandwich plates and shells: the in-plane stress discontinuity at the interfaces between the core and the faces can be reduced or eliminated, the maximum values of displacements and stresses are reduced with the use of FGM inter-layers. In order to introduce such FGM layers, some parameters must be correctly chosen: opportune values of the FGM-layer thickness

(h_{FGM}) and appropriate laws for the FGM elastic properties (exponent κ) permit remarkable improvements to be obtained in the static response of such structures. The choice of the FGM-layer thickness and the elastic property law (κ-h_{FGM} effect) depends on the variable (displacement, in-plane stresses or out-of-plane stresses) that one wants to modify and on its position in the thickness direction z.

REFERENCES

1. M. Koizumi, The concept of FGM, Ceramic Transactions, Functionally Gradient Materials, vol. 34, pp. 3–10, 1993.
2. M. Koizumi, FGM Activities in Japan, Composites Part B: Engineering, vol. 28, no. 1–2, pp. 1–4, 1997.

3. B. Birman and L.W. Byrd, Modeling and Analysis of Functionally Graded Materials and Structures, Appl. Mech. Rev., vol. 60 no. 5, 195–216, 2007.

4. M.-J. Pindera, S.M. Arnold, J. Aboudi, et al., Use of Composites in Functionally Graded Materials, Compos. Eng., vol. 4, no. 1, pp. 1–145, 1994.

5. M.-J. Pindera, J. Aboudi, S.M. Arnold, et al., Use of Composites in Multi-Phased and Functionally Graded Materials, Compos. Eng., vol. 5, no. 7, pp. 743–974, 1995.

6. S. Suresh and A. Mortensen, Fundamentals of Functionally Graded Materials: Processing and Thermomechanical Behavior of Graded Metals and Metal-Ceramic Composites, IOM Communications Ltd, 1998, London (UK).

7. M. Kashtalyan, Three-Dimensional Elasticity Solution for Bending of Functionally Graded Rectangular Plates, Eur. J. Mech. A Solid., vol. 23, no. (5), pp. 853–864, 2004.

8. V.P. Plevako, On the Theory of Elasticity of Inhomogeneous Media, J. Appl. Math. Mech., vol. 35, no. (5), pp. 806–813, 1971.

9. M. Kashtalyan and M. Menshykova, Three-Dimensional Elasticity Solution for Sandwich Panels with a Functionally Graded Core, Compos. Struct., vol. 87, no. (1), pp. 36–43, 2009.

10. E. Pan, Exact solution for Functionally Graded Anisotropic Elastic Composite Laminates, J. Compos. Mater., vol. 37, no. (21), pp. 1903–1920, 2003.

11. A.N. Stroh, Steady State Problems in Anisotropic Elasticity, J. Math. Phys., vol. 41, pp. 77–103, 1962.

12. N.J. Pagano, Exact Solutions for Composite Laminates in Cylindrical Bending, J. Compos. Mater., vol. 3, pp. 398–411, 1969.

13. N.J. Pagano, Exact Solutions for Rectangular Bidirectional Composites and Sandwich Plates, J. Compos. Mater., vol. 4, pp. 20–34, 1970.

14. M. Bayat, M. Saleem, B.B. Sahari, et al., Analysis of Functionally Graded Rotating Disks with Variable Thickness, Mech. Res. Comm., vol. 35, no. (5), pp. 283–309, 2008.

15. A.M. Zenkour, Generalized Shear Deformation Theory for Bending Analysis of Functionally Graded Plates, Appl. Math. Model., vol. 30, no. (1), pp. 67–84, 2006.

16. A.J.M. Ferreira, R.C. Batra, C.M.C. Roque, et al., Static Analysis of Functionally Graded Plates Using Third-Order Shear Deformation Theory and a Meshless Method, Compos. Struct., vol. 69, no. (4), pp. 449–457, 2005.

17. F. Ramirez, P.R. Heyliger, and E. Pan, Static Analysis of Functionally Graded Elastic Anisotropic Plates Using a Discrete Layer Approach, Composites Part B: Engineering, vol. 37, no. (1), pp. 10–20, 2006.

18. S.-H. Chi and Y.-L. Chung, Mechanical Behavior of Functionally Graded Material Plates Under Transverse Load. Part I: Analysis, Int. J. Solid Struct., vol. 43, no. (13), pp. 3657–3674, 2006.

19. S.-H. Chi and Y.-L. Chung, Mechanical Behavior of Functionally Graded Material Plates Under Transverse Load. Part II: Numerical Results, Int. J. Solid Struct., vol. 43, no. (13), pp. 3675–3691, 2006.

20. L.F. Qian, R.C. Batra, and L.M. Chen, Static and Dynamic Deformations of Thick Functionally Graded Elastic Plates by Using Higher-Order Shear and Normal Deformable Plate Theory and Meshless Local Petrov-Galerkin Method, Composites Part B: Engineering, vol. 35, no. (6–8), pp. 685–697, 2004.

21. S.N. Athuri and T. Zhu, A new Meshless Local Petrov-Galerkin (MLPG) Approach in Computational Mechanics, Computational Mechanics, vol. 22, pp. 117–127, 1998.

22. S.S. Vel and R.C. Batra, Three-Dimensional Exact Solution for the Vibration of Functionally Graded Rectangular Plates, J. Sound Vibr., vol. 272, no. (3–5), pp. 703–730, 2004.

23. R.C. Batra and J. Jin, Natural Frequencies of a Functionally Graded Anisotropic Rectangular Plate, J. Sound Vibr., vol. 282, no. (1–2), pp. 509–516, 2005.

24. E. Carrera, A Class of Two-Dimensional Theories for Multilayered Plates Analysis, Accademia delle Scienze di Torino, Memorie Scienze Fisiche, vol. 19–20, pp. 1–39, 1995.

25. E. Carrera, Theories and finite Elements for Multilayered Plates and Shells: A unified Compact Formulation with Numerical Assessments and Benchmarking, Archiv. Comput. Method Eng., vol. 10, no. (3), pp. 215–296, 2003.

26. E. Reissner, On a Certain Mixed Variational Theory and a Proposed Application, Int. J. Numer. Meth. Eng., vol. 20, no. (7), pp. 1366–1368, 1984.

27. E. Carrera, Evaluation of Layerwise Mixed Theories for Laminated Plates Analysis, AIAA J., vol. 36, no. (5), pp. 830–839, 1998.

28. E. Carrera, S. Brischetto, and A. Robaldo, Variable Kinematic Model for the Analysis of Functionally Graded Material Plates, AIAA J., vol. 46, no. (1), pp. 194–203, 2008.

29. S. Brischetto and E. Carrera, Advanced Mixed Theories for Bending Analysis of Functionally Graded Plates, Comput. Struct., in press, available on line on May 2008.

30. S. Brischetto, Classical and Mixed Advanced Models for Sandwich Plates Embedding Functionally Graded Cores, J. Mech. Mater. Struct., vol. 4, no. (1), pp. 13–33, 2009.

31. A.L. Cauchy, Sur l'équilibre et le Mouvement d'une Plaque Solide, Exercise des Mathématique, vol. 3, pp. 381–412, 1828.

32. S.D. Poisson, Mémoire sur L'équilibre et le mouvement des Corps éLastique, Mémoires de l'Académie des Sciences des Paris, vol. 8, pp. 357–570, 1829.

33. G. Kirchhoff, Über das Gleichgewicht und die Bewegung Einer Elastishen Scheibe, Journal fur die reine und Angewandte Math, vol. 40, pp. 51–88, 1850.

34. E. Reissner, The Effect of Transverse Shear Deformation on the Bending of Elastic Plates, J. Appl. Mech., vol. 12, no. 2, pp. 69–77, 1945.

35. R.D. Mindlin, Influence of Rotatory Inertia and Shear in flexural Motions of Isotropic Elastic Plates, J. Appl. Mech., vol. 18, pp. 31–38, 1951.

36. A.W. Leissa, Vibration of Shells, NASA SP-288, Washington, D.C. (USA), 1973.

37. A.W. Leissa, Vibration of Plates, NASA SP-160, Washington, D.C. (USA), 1969.

38. E. Carrera and S. Brischetto, Analysis of Thickness Locking in Classical, refined and Mixed Multilayered Plate Theories, Compos. Struct., Vol. 82, no. 4, pp. 549–562, 2008.

39. E. Carrera and S. Brischetto, Analysis of Thickness Locking in Classical, refined and Mixed Theories for Layered Shells, Compos. Struct., vol. 85, no. 1, pp. 83–90, 2008.

40. E. Carrera, Historical Review of Zig-Zag Theories for Multilayered Plates and Shells, Appl. Mech. Rev., vol. 56, no. 3, pp. 287–309, 2003.

41. H. Murakami, Laminated Composite Plate Theory with Improved In-Plane Responses, ASME Proceedings of PVP Conference, PVP-98-2, June 1985, New Orleans (USA).

42. H. Murakami, Laminated Composite Plate Theory with Improved In-Plane Responses, J. Appl. Mech., vol. 53, pp. 661–666, 1986.

43. J.N. Reddy, Mechanics of Laminated Composite Plates and Shells. Theory and Analysis, CRC Press, New York (USA), 2004.